RSC Advances

ROYAL SOCIETY OF CHEMISTRY

www.rsc.org/advances

RSC Advances

REVIEW

Fluorescent Graphene Quantum Dots for Biosensing and Bioimaging

Zetan Fan, Shuhua Li, Fanglong Yuan and Louzhen Fan*

5 Fluorescent carbon-based nanomaterials, including carbon dots (C-Dots) and the emerging graphene quantum dots (GQDs) are attracting increasing interest in the field of biosensing and bioimaging for their high aqueous solubility, stable photoluminescence (PL), low cytotoxicity, good biocompatibility as well as superior resistance to photobleaching. Compared with C-Dots, the quasi zero-dimensional (0D) GQDs with a few atomic layers can exhibit strong PL without passivation. With these extraordinary properties, 10 GQDs are suitable alternatives as both a versatile platform for biosensing and a promising class of bioimaging probes. In this review, we introduce the synthesis, structure, PL properties and currently available applications of GQDs in biosensing and bioimaging field. We hope this review will provide critical insights to inspire more exciting researches on GQDs for biological applications to better realize the potential of the intriguing GQDs in the near future.

1. Introduction

15 Graphene, a novel single-atom-thick and two-dimensional (2D) nano-graphitic carbon sheet, exhibits characteristics including large surface area, high carrier transport mobility, superior mechanical flexibility and excellent thermal and chemical 20 stability, which are suitable for various applications in optoelectronic devices, energy-storage media and drug-delivery vehicles.[1-4] Since graphene is a zero-bandgap semiconductor, no optical photoluminescence (PL) is observed in pristine form, which limits its application in optoelectronics. However, both 25 theoretical and experimental studies show that the band gap of graphene can be tuned by converting 2D graphene sheets into zero-dimensional (0D) graphene quantum dots (GQDs).[5-8] Due to quantum confinement and edge effects, GQDs, as a new kind of

quantum dots (QDs), have attracted tremendous research interest 30 due to their high aqueous solubility, stable PL, low cytotoxicity, good biocompatibility as well as superior resistance to photobleaching compared with traditional semiconductor QDs and organic dyes.[9,10]

Another example of 0D fluorescent carbon-based nanomaterials, 35 carbon dots (C-Dots) have also attracted much attention in recent years.[11-13] Though GQDs are even considered as a kind of C-Dots, some differences should be pointed out. C-Dots are either amorphous or crystalline,[14] while GQDs clearly possess graphene lattices inside the dots produced from graphene-based starting 40 materials or the rigid synthetic chemistry of graphene-like smaller polycyclic aromatic hydrocarbon molecules.[15,16] Unlike the quasi-spherical C-Dots, GQDs with a few atomic layer graphene sheets can exhibit strong PL without passaivation.[17] Moreover, the unique PL properties of GQDs can be effectively 45 tuned by doping heteroatoms to the π-conjugated system.[18-20]

50

Department of Chemistry, Beijing Normal University, Beijing, 100875, China. E-mail: lzfan@bnu.edu.cn

Zetan Fan received her BS degree in chemistry from Xinyang Normal University in 2011. She is currently a Ph.D. student with Prof. Louzhen Fan at Beijing Normal University. Her research interests involve preparation and functionalization of carbon nanomaterials for biological applications.

Shuhua Li received her BS degree in chemistry from Shanxi Datong University in 2012. Currently, she is a Master student in the group of Prof. Louzhen Fan at Beijing Normal University. Her research interests focus on GQDs-based composites for electrochemical applications and biosensors.

55

With these extraordinary properties, GQDs are suitable alternatives as both a versatile platform for biosensing and a promising class of bioimaging probes. To date, various GQDs-based probes for the detection of ions, biomolecules and small
[5] organic molecules with aromatic structures have been designed,[21] and biomarkers based on blue and green fluorescent GQDs have been widely used.[22] However, much work is still needed to explore the full potential of these nanomaterials for

developing advanced smart sensors and biomarkers.
[10] In this review, we introduce the synthesis, structure, PL properties and currently available applications of GQDs in biosensing and bioimaging field. We hope this review will provide critical insights to inspire more exciting researches on GQDs for biological applications to better realize the potential
[15] of the intriguing GQDs in the near future.

Table 1 A brief summary of the typical synthetic methods for GQDs

Methods	Subclassification	Raw materials	Size (nm)	Color	Quantum yield (QY, %)	Ref.
Top-down	Acid oxidation	Carbon black	15-18	Green, yellow	4.04, 2.09	23
		Carbon fibers	1-4	Blue, green, yellow		24
		Coal	2.96±0.96	Green		25
	Hydrothermal	GO	1.5-5	Green	7.5	26
		GO	5-13	Blue	6.9	17
	Solvothermal	GO	~3	Green	31	27
		GO	3-5	Blue, Green	29–19	28
	Microwave	GO	2-7	Blue, Green		29
		GO	3	Blue	22.9	30
	Sonication	Graphene	3-5	Blue	3.4	10
	Electrochemistry	Graphite rod	5-10	Yellow	14	33
		Graphite rod	3-7	Green, yellow	13	19
		Graphite rod	3	Green	10.6	20
		Graphene	~3.0	Blue	10	35
	Chemical exfoliation	Multi-wall carbon nanotubes (MWCNTs)	20	Blue	6.53	36
		Graphite nanoparticles	4	Blue		37
Bottom-up	Hydrothermal	Pynene	3.6±1.2	Green	23	40
		Polythiophene derivatives	2-6	Red	5.4	41
	Microwave-assist pyrolysis	Glycerol	1-5	Green		45
	Catalyzed cage-opening	C_{60}	2.7-10			46
	Precursor pyrolysis	L-Glutamic acid	4.66±1.24	Blue	54.5	44
		Citric acid	15	Blue	9.0	42
		Glucose	1.6-21	Blue, UV	7-11	43

[20]

Fanglong Yuan obtained his BS in Applied Chemistry in Beijing University of Chemical Technology in 2013. He is now a Ph.D. student under the supervision of Prof. Louzhen Fan at Beijing Normal University. His research is centered on the synthesis and biological applications of carbon nanomaterials.

[25]

Louzhen Fan is now a chemistry professor of Department of Chemistry, Beijing Normal University. She received her Ph.D. in physical chemistry in 1998 under the supervision of Prof. Daoben Zhu and Prof. Yongfang Li from Institute of Chemistry, the Chinese Academy of Sciences, Beijing. Her research

interests are focused on the synthesis of novel carbon and metal nanomaterials and their applications in biology and energy.

2. Synthesis, structure and PL properties of GQDs

2.1 Synthesis and structure

Up to now, the synthesis of GQDs with tunable size can be generally divided into two strategies: top-down and bottom-up
5 methods. The typical methods are listed in Table 1. The top-down routes are implemented *via* either physical or chemical techniques to cut down large graphene or graphene oxide (GO) sheets, carbon nanotubes (CNTs), carbon fibers or graphite into small pieces of graphene sheets while in the bottom-up methods,
10 GQDs are controllably prepared by stepwise reactions of small molecules. For top–down approaches, acidic oxidation,[23-25] hydrothermal[17,26] or solvothermal,[27,28] microwave-assisted,[29,30] sonication-assisted,[31] electrochemical,[12,19,20,32-35] chemical exfoliation,[36,37] photo-fenton reaction[15] methods have been used
15 to synthesize GQDs. Conversely, the bottom-up methods offer us exciting opportunities to control the GQDs with well-defined molecular size, shape and properties. Stepwise solution chemistry methods using benzene derivatives,[38-41] precursor pyrolysis,[42-44] microwave-assisted hydrothermal treatment of carbohydrates,[45]
20 ruthenium-catalyzed cage-opening of fullerenes[46] and carbonization of hexaperihexabenzocoronene (HBC)[16] have been utilized to prepare GQDs successfully.

In general, the average sizes of GQDs are mostly below 10 nm, and the largest diameter of GQDs reported so far is 60 nm.[16]
25 Similar to the size, the height of GQDs depends on the preparation methods, mostly ranging from 0.5 to 5 nm. However, the heights of GQDs prepared through different methods don't monotonously relate to their sizes. Most of GQDs consist of no more than 5 layers, and a great deal of monolayer GQDs have
30 been prepared successfully.[23,26,33] GQDs prepared by our group *via* electrochemical exfoliation of graphite followed by room temperature reduction with hydrazine (N_2H_4) were uniform and monodisperse (Fig. 1a, b), with an average diameter of 5 to 10 nm (Fig. 1c) and a topographic height below 0.5 nm (Fig. 1d, e),
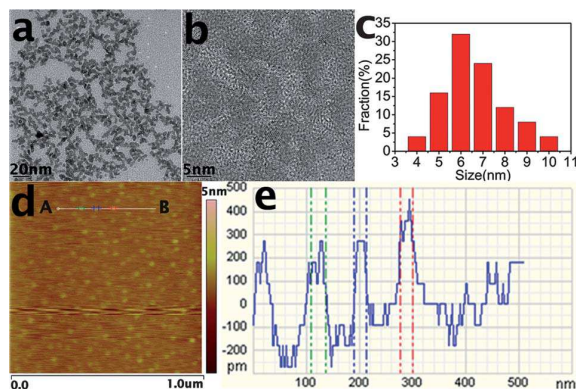35 mostly consisting of a single graphene layer.[33]

Fig. 1 TEM (a) and HRTEM (b) images and size distribution (c) of GQDs. (d) AFM image of the GQDs deposited on freshly cleaved micasubstrates. (e) Height profile along the line from A to B in (d). Reprinted with
40 permission from: ref. 33, copyright 2012 Royal Society of Chemistry.

The high resolution transmission electron microscopy (HRTEM) images of GQDs feature two kinds of lattice fringes, namely (002) interlayer spacing and (1120) in-plane lattice spacing. The former centered at about 0.34 nm has been observed
45 from GQDs prepared by acidic oxidation of carbon black[23] and

electrochemical cutting method,[32] the latter mostly centered at about 0.24 nm has been observed from GQDs synthesized *via* acidic oxidation from carbon fiber,[24] hydrothermal treatment[29] and photo-fenton reaction,[15] excepting for 0.21 nm (Fig. 2a) *via*
50 hydrothermal cutting strategy.[26] Interestingly, the two kinds of lattice fringes (Fig. 2b) have been simultaneously been observed in the case of electrochemical method from MWCNTs.[34]
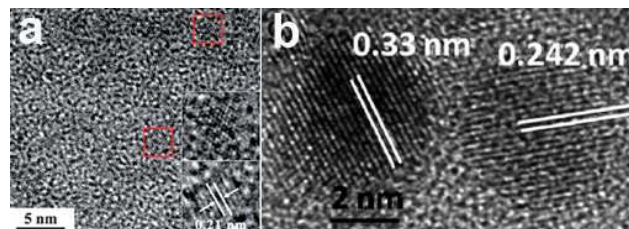

Fig. 2 (a) TEM image of GQDs. (b) Fringe patterns of GQDs. Reprinted
55 with permission from: (a): ref. 26, copyright 2012 Royal Society of Chemistry, (b): ref. 34, copyright 2012 Wiley-VCH.

GQDs are generally composed of a series of surface groups, such as carboxyl, hydroxyl and epoxy groups.[9,10] Fourier transform infrared spectroscopy (FTIR) and X-ray photoelectron
60 spectroscopy (XPS) are commonly adopted to analyze their components. For sulfur-doped GQDs (S-GQDs) prepared by electrolysis of graphite in sodium p-toluenesulfonate aqueous solution,[20] the XPS survey spectrum (Fig. 3a) showed dominant graphitic C1s peak at 284 eV, S2p peak at 167 eV and O1s peak
65 at 531 eV. The presence of C=C, C-O, C=O, C-S bonds indicated that GQDs were functionalized with hydroxyl, carbonyl, carboxyl and epoxy groups, and the high-resolution S2p spectrum confirmed the successful incorporation of S atoms into GQDs (Fig. 3b, c). The results were further confirmed by the
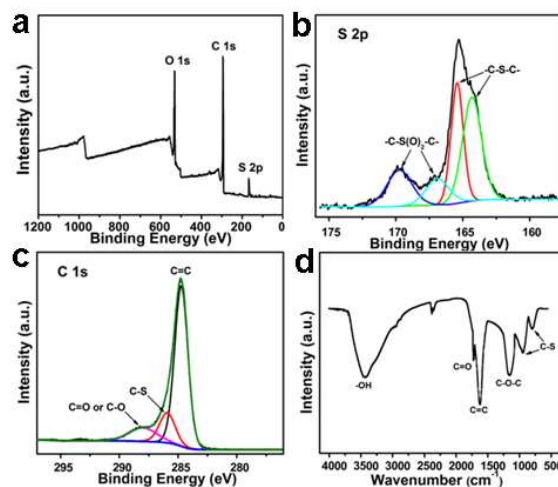70 corresponding FTIR spectrum (Fig. 3d).

Fig. 3 XPS (a) S2p (b) C1s (c) and FTIR (d) spectra of S-GQDs. Reprinted with permission from: ref. 20, copyright 2014 American Chemical Society.

75 Raman spectroscopy is also a powerful and non-destructive tool for the characterization of GQDs. The G band is assigned to the E_{2g} vibration modes of the aromatic domains, whereas the D band arises from the breathing modes of graphitic domains. Traditionally, the intensity ratio of disorder D to crystalline G
80 (I_D/I_G) is used to compare the structural order between crystalline

and amorphous graphitic systems. The I_D/I_G values of GQDs vary significantly depending on the preparation methods. The electrochemically prepared boron-doped GQDs (B-GQDs) from high purity graphite rods have a high I_D/I_G value of 1.23,[19] indicating numerous defects on the B-GQDs.

2.2 Absorbance and PL properties

For the UV-vis absorption spectrum of GQDs, two typical peaks can be observed: a peak at around 230 nm assigned to π-π* transition of aromatic C=C bonds and a shoulder at about 300 nm due to n-π* transition of C=O bonds.[23,33,37] The most fascinating feature of GQDs is their PL. Variously sized GQDs with deep ultraviolet,[38] blue,[15,17,24,28,31,34,36] green,[12,23,26-28] yellow,[33] and red[41] colors have been prepared *via* different synthetic approaches. The PL mechanism may derive from intrinsic state emission and defect state emission,[47] which arise from quantum confinement effect, emissive traps, excitons of carbon, aromatic structures, oxygen-containing groups, free zigzag sites and edge defects.[48-50]

The PL of GQDs are influenced by many factors, such as size,[16,23,24,51] excitation wavelength,[52,53] pH,[17,24,52,53] solvent polarity,[52,54] surface oxidation degree,[30,53] surface functionalizations[28,51] and heteroatom doping.[19,20] Three kinds of GQDs with different sizes of 1-4, 4-8, and 7-11 nm *via* varying the reaction temperatures, emitted different PL changing from blue and green to yellow (Fig. 4a, b).[24] GQDs prepared *via* acidic oxidation from carbon black exhibited PL transition from green to yellow as their sizes increased from 15 to 18 nm.[23] The size-dependent PL of GQDs mainly attributed to the quantum confinement effect. However, it is worth noting that the size-independent PL of the GQDs (Fig. 4c) has also been observed from glucose carbonization,[43] due to the surface state emission. The largest GQDs prepared from unsubstituted hexa-*peri*-hexabenzocoronene (HBC) also showed blue PL (Fig. 4d),[16] which could be ascribed to the zigzag edge sites and defect effect.[17]
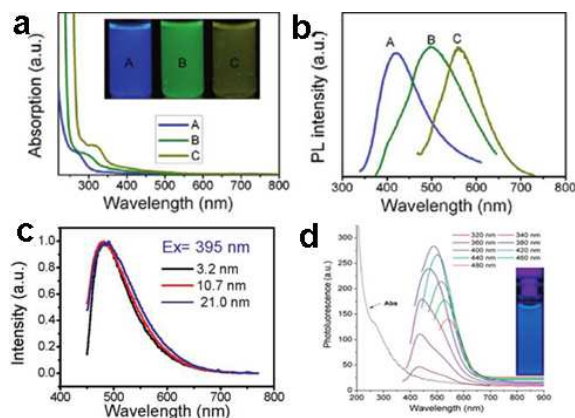

Fig. 4 (a) UV-vis spectra of GQDs A, B, and C, corresponds to synthesized reaction temperature at 120, 100, and 80 ºC, respectively. Inset of panel is a photograph of the corresponding GQDs under UV light with 365 nm excitation. (b) PL spectra of GQDs with different emission color excited at 318, 331, and 429 nm, respectively. (c) The normalized PL spectra of the GQDs with various sizes. (d) UV-vis absorption and PL emission spectra of GQDs. Reprinted with permission from: (a) and (b): ref. 24, copyright 2012 American Chemical Society, (c): ref. 43, copyright 2012 American Chemical Society, (d): ref. 16, copyright 2011 American Chemical Society.

GQDs prepared *via* hydrothermal method exhibited excitaion-dependent PL properties[17] (Fig. 5a) which might result from different size or emissive sites.[54,55] Meanwhile, the excitation-independent PL behavior has also been reported (Fig. 5b).[31,33,42] This could be explained by the high uniformity emissive sites contained in GQDs. Interestingly, the PL of GQDs has also been found to be sensitive to solvent and pH. The emission peak of GQDs synthesized *via* solvothermal method shifted from 475 to 515 nm in THF, acetone, DMF, and water, respectively (Fig. 5c).[54] Under alkaline conditions, the hydrothermally synthesized GQDs emitted strong blue PL while under acidic conditions it was nearly completely quenched (Fig. 5d). When pH was switched repeatedly between 13 and 1, the PL intensity varied reversibly.[17] In addition, the pH had nearly no influence on the PL wavelength, but just affected the PL intensities of GQDs, which was also observed in GQDs with emissive zigzag sites.[24,26]
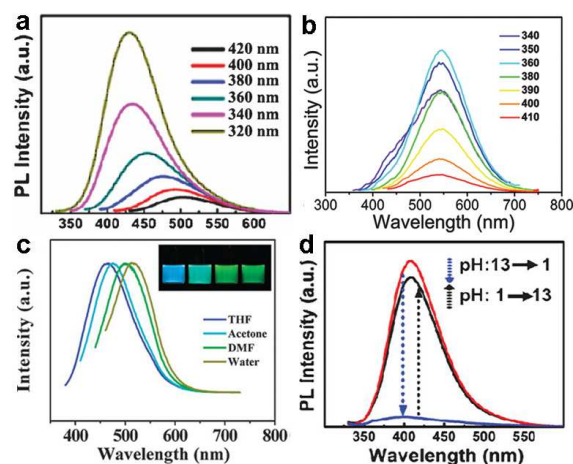

Fig. 5 (a) PL spectra of the GQDs at different excitation wavelengths. (b) PL spectra of the GQDs at different excitation wavelengths. (c) Effect of solvents on the fluorescence of GQDs. (d) pH-dependent PL spectra when pH is switched between 13 and 1. Reprinted with permission from: (a) and (d): ref. 17, copyright 2010 Wiley-VCH, (b): ref. 33, copyright 2012 Royal Society of Chemistry, (c): ref. 54, copyright 2011 Royal Society of Chemistry.

Doping GQDs with heteroatoms could effectively modulate their band gap and electronic density, enhancing chemical activity and QY of GQDs for practical applications, which were proved through theoretical calculations and detailed experiments.[17,19,20,38] B-GQDs gave rise to rich PL owing to their peculiar interaction with the surrounding media of borax (Fig. 6a, b)[19] and S-GQDs exhibited bright green PL (Fig. 6c).[20] Upconversion PL, another exciting feature of GQDs, was reported by many groups,[47,49,56] but some results were artificial. Gan *et al.* revealed that the upconversion PL in GQDs under excitation from a xenon lamp was excited by the second-order diffraction light of wavelength λ/2 coexisting in the excitation light of wavelength λ. The real upconversion from GQDs was obtained under excitation with a femtosecond pulsed laser (Fig. 6d).[57]

The QY of GQDs varies with the fabrication method and the surface chemistry involved. For the unpassivated GQDs, their QYs are always low, due to the carboxylic and epoxide groups contained in GQDs acting as the non-radiative electron-hole recombination centers.[58] Therefore, the removal of these oxygen-

containing groups may improves the QY, either by reduction or surface passivation.[59] Li *et al.* improved the QY of GQDs from 11.7 to 22.9% by gentle reduction with $NaBH_4$.[30] Our group obtained yellow fluorescent GQDs with a relative high QY about 14% by reduction with N_2H_4.[33] Tetsuka *et al.* prepared amino-functionalized GQDs with QY ranging from 29 to 19%, which decreased with quantity of amine functionalization.[28]
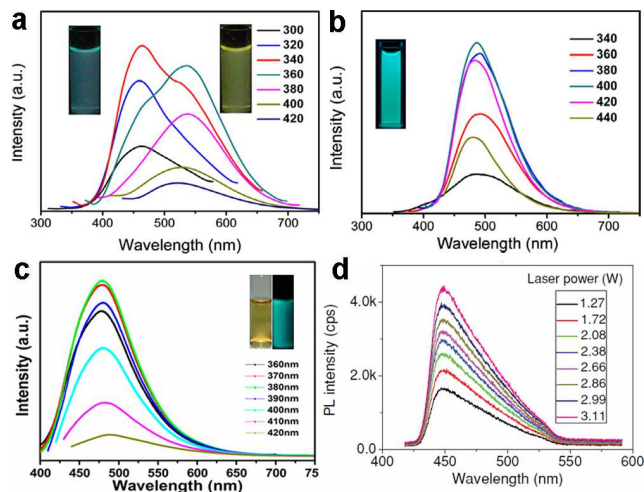
Fig. 6 PL spectra of the B-GQDs aqueous solution in the absence (a) and presence (b) of borax. (c) PL spectra of S-GQD. (d) Upconversion photoluminescence spectra obtained from GQDs under excitation of a femtosecond pulsed laser at 800 nm. Reprinted with permission from: (a) and (b): ref. 19, copyright 2014 Elsevier, (c): ref. 20, copyright 2014 American Chemical Society, (d): ref. 57, copyright 2013 Wiley-VCH,

3. Biosensing

In view of the high aqueous solubility, stable PL, low cytotoxicity, good biocompatibility, superior resistance to photobleaching as well as unique electrochemical and electrochemiluminescence (ECL) emission properties of GQDs, PL, electrochemical and ECL biosensors have been explored to detect ions, biomaterials, and small organic molecules with aromatic structures.

3.1 PL biosensors

Various GQDs-based PL sensors have been fabricated with either signal-off or signal-on process. Recently, our group presented a novel PL sensor using S-GQDs for the detection of Fe^{3+} in human serum samples (Fig. 7a).[20] Doping GQDs with S atom could effectively modulate the band gap and electronic density of GQDs, which promoted the coordination interaction between Fe^{3+} and phenolic hydroxyl groups of S-GQDs, leading to significant PL quenching. Such PL probe exhibited highly sensitive and selective detection of Fe^{3+} in the concentration range of 0.01-0.70 μM, and the limit of detection (LOD) was as low as 4.2 nM. Taking advantage of the PL quenching of GQDs, a turn-off sensor for Ag^+ and biothiol detection was developed by Ran *et al.*[60] The formation of Ag nanoparticles (AgNPs) on GQDs was able to quench the PL of GQDs and the addition of biothiols could cause a further turn-off phenomenon due to their strong interaction through the formation of Ag-S bonds. The LOD was 3.5 nM for Ag^+, 6.2 nM for cysteine (Cys), 4.5 nM for homocysteine (Hcy) and 4.1 nM for glutathione (GSH) in the

range 0-100 nM. He *et al.* reported a glucose biosensor *via* the PL quenching of hemin-functionalized GQDs.[61] According to the surface quenching states (SQS) induced mechanism, 3-aminobenzeneboronic acid functionalized GQDs (APBA-GQDs) were also used for glucose detection by Qu *et al.*[62] In addition, Wang *et al.* developed a simple PL off assay for the activity of protein kinase CK2 based on the selective aggregation of phosphorylated peptide-GQD conjugates triggered by Zr^{4+} coordination.[63] When the substrate peptide was phosphorylated by CK2, the introduced Zr^{4+} could serve as a linkage between the phosphorylated sites of phosphopeptides *via* the multi-coordinative interactions between Zr^{4+} and phosphate groups, resulting in extensive aggregation of the GQDs and effective PL quenching (Fig. 7b), thus the activity of protein kinase could be facilely monitored with an LOD of 0.03 unit mL^{-1}.
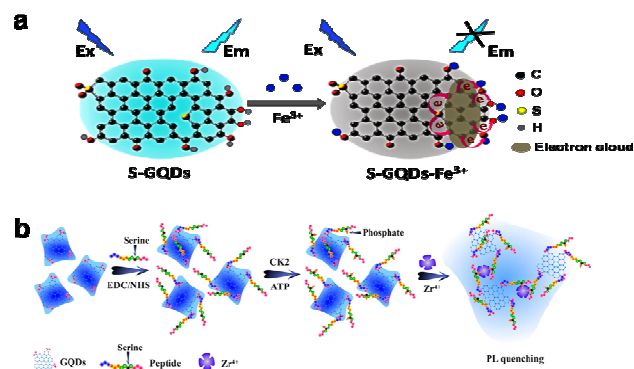
Fig. 7 (a) Schematic illustration of the PL quenching mechanism of the S-GQDs in the presence of Fe^{3+}. (b) Schematic representation of the CK2 kinase assay based on the aggregation and PL quenching of phosphorylated peptide-GQD conjugates *via* Zr^{4+} linkages. Reprinted with permission from: (a): ref. 20, copyright 2014 American Chemical Society, (b): ref. 63, copyright 2013 American Chemical Society.

Apart from the signal-off PL sensors described above, signal-on PL sensors have been designed as well.[19,64-69] An aggregation-induced PL increasing sensor for label-free detection of glucose was proposed by Zhang *et al.*[64] The reaction of the two cis-diol units in glucose with the two boronic acid groups on the boron-doped GQDs (BGQDs) surfaces created structurally rigid BGQDs-glucose aggregates, restricting the intramolecular rotations and thus resulting in a great boost in the PL intensity (Fig. 8a). In another study, Li *et al.* designed a glucose sensing system using anionic GQDs and a cationic boronic acid-substituted bipyridinium salt (BBV).[65] The pristine GQDs acted as luminescent reporting units, while BBV served as a PL quencher and a glucose receptor simultaneously. It was postulated that the electrostatic attraction between GQDs and BBV resulted in the formation of a ground-state complex which facilitated the excited-state electron transfer from GQDs to bipyridinium and quenched the PL intensity of the GQDs. When glucose was added to the system, the boronic acids were converted to tetrahedral anionic glucoboronate esters, which effectively neutralized the net charge of the cationic bipyridinium, greatly diminishing its quenching efficiency, and the PL intensity of GQDs recovered. Li *et al.* demonstrated a label-free PL signal-on assay for the detection of trypsin with an LOD of 33 ng mL^{-1} based on cytochrome c (Cyt c)-induced self-assembled GQDs.[66] Cyt c which is rich in Fe^{3+} could quench the

fluorescence of GQDs. When trypsin was present, Cyt c was cleaved into smaller fragments on the C-terminal side of arginine and lysine residues, and Fe^{3+} in Cyt c was reduced to Fe^{2+} with the aid of the digestive enzyme. Thus the cleaved Cyt c was unable to quench the PL of GQDs, which resulted in the restoration of PL. Moreover, trypsin cleaved the peptide bonds of Cyt c to gave lysine and arginine residues, both of which chemically reduced GQDs into reduced-GQDs (r-GQDs), inducing a subsequent increase in PL intensity. Liu *et al.* proposed a PL "off-to-on" mechanism of glutathione-functionalized GQDs (GQDs@GSH) for the assay of adenosine triphosphate (ATP).[67] Fe^{3+} quenched the fluorescence of GQDs@GSH by electron transfer and then were disassociated from GQDs@GSH by the phosphate ions through the strong interactions, which resulted in the restoration of PL. Since ATP was the major phosphate-containing metabolite in cell lysates and blood serum, the proposed sensing assay was successfully applied to estimate ATP level in cell lysates and blood serum. Wu *et al.* designed a PL turn-on sensor for biothiols detection and the LOD for GSH, Cys and Hcy were 5 nM, 2.5 nM and 5 nM, respectively.[68] Hg^{2+} could efficiently quench the blue PL of GQDs and biothiols selectively bonded to Hg^{2+} through Hg-S bonding interactions to recover the PL of GQDs. Our group demonstrated B-GQDs used as PL turn-on sensor for detecting Al^{3+} (Fig. 8b).[19] With increasing Al^{3+} concentration from 0 to 100 μM, the PL intensity of B-GQDs was enhanced linearly. The LOD of B-GQDs towards Al^{3+} was estimated as 3.64 μM, which met the limit for drinking water according to the World Health Organization standard (7.41 μM).
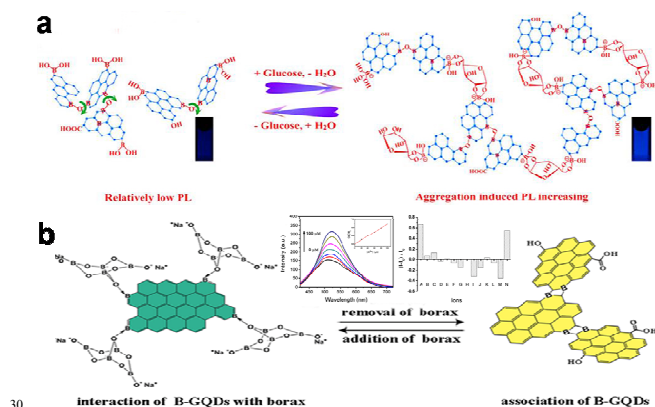

Fig. 8 (a) Proposed "Aggregation-Induced PL Increasing" Mechanism for the Glucose-Specific Sensing by BGQDs. (b) The structure illustration of B-GQDs in the presence (left) and absence (right) of borax, respectively. Inset: PL emission spectra of B-GQDs aqueous solution upon adding different concentrations of Al^{3+} ions at 405 nm excitation and maximum luminescent response of B-GQDs upon addition of different metal ions (100 μM) listed from left to right: (A) Al^{3+}, (B) Ag^+, (C) Na^+, (D) K^+, (E) Mg^{2+}, (F) Ca^{2+}, (G) Ba^{2+}, (H) Cd^{2+}, (I) Pb^{2+}, (J) Fe^{2+}, (K) Zn^{2+}, (L) Fe^{3+}, (M) Cr^{3+} and (N) $Al^{3+} + Na^+ + K^+ + Mg^{2+} + Ca^{2+} + Ba^{2+} + Fe^{3+}$. Reprinted with permission from: (a): ref. 64, copyright 2014 American Chemical Society, (b): ref. 19, copyright 2014 Elsevier.

Since π-π stacking interaction between graphene and GQDs could bring them into luminescence resonance-energy transfer (LRET) proximity and lead to PL quenching of GQDs, a series of LRET sensors were developed.[70-72] Zhao *et al.* presented a LRET immunosensor using graphene as acceptor and mouse anti-human immunoglobulin G (mIgG, antibody) conjugated-GQDs as donor

for the sensitive detection of human immunoglobulin G (IgG, antigen) with an LOD of 10 ng mL^{-1}.[70] When adding graphene into the mIgG-GQDs solution, both the π-π stacking interaction between graphene and GQDs and the nonspecific binding interaction between mIgG and the graphene surface brought graphene and GQDs into LRET proximity to facilitate the PL quenching of GQDs. The addition of human IgG would bind the mIgG due to the specific antibody-antigen interaction, which effectively increased the distance between mIgG-GQDs and graphene surface, thus hindering the LRET process and then producing a restoration of PL. Qian *et al.* established a PL sensing platform for DNA detection by regulating the interaction between the reduced GQDs (rGQD) labeled DNA probe and GO (Fig. 9).[71] When ssDNA-rGQDs probe was absorbed on the surface of GO, both electrostatic attractions and π-π stacking interactions between ssDNA-rGQDs and the GO surface resulted in substantial PL quenching of ssDNA-rGQDs. Upon the addition of target DNA (tDNA), the tDNA could capture the ssDNA-rGQDs in the assembled ssDNA-rGQDs/GO to produce dsDNA-rGQDs through specific base pairing, leading to the liberation and detachment of the dsDNA-rGQDs from the GO and PL recovery from the free dsDNA-rGQDs. The established method for DNA detection had a broad linear range of 6.7-46.0 nM with an LOD of 75.0 pM. Furthermore, Qian *et al.* constructed a dual-functional biosensor for simultaneous detection of DNA and bovine α-thrombin by taking advantage of the intense dual-color PL of GQDs, efficient quenching effect of GO, specific recognition between probes and targets, and unique interaction between GQDs and GO.[72] Like graphene and GO, CNTs were also used as acceptor in the LRET process for DNA detection by Qian *et al.*[73] The specific PL "on-off-on" process originated from PL quenching owing to LRET between GQDs-labeled probe and CNTs and subsequent PL recovery due to liberation of free double-stranded DNA probe was employed to achieve quantitative analysis of target DNA.
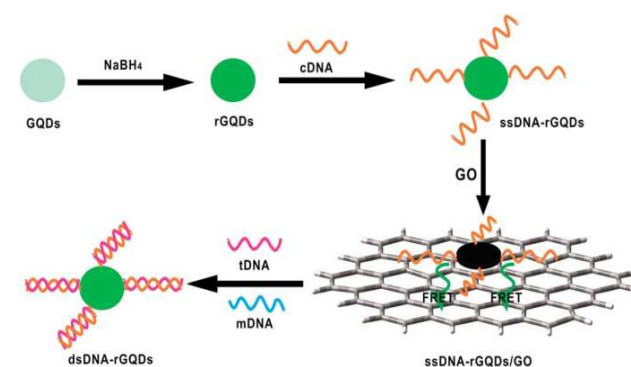

Fig. 9 Schematic illustration of a universal PL sensing platform for the detection of DNA based on LRET between GQDs and GO. Reprinted with permission from ref. 71, copyright 2014 Royal Society of Chemistry.

3.2 Electrochemical biosensors

GQDs, which can act as multivalent redox species using cyclic voltammetry (CV), chronoamperometry (CA) and differential pulse voltammetry (DPV) measurements, present exciting opportunities for building electrochemical sensors.[74-91] The first electrochemical sensor was designed for the detection of ssDNA by Zhao *et al.*[74] The probe ssDNA (ssDNA-1) immobilized on

GQDs inhibited the electron transfer effect between the electro-active species $[Fe(CN)_6]^{3-/4-}$ and the electrode *via* electrostatic repulsion, resulting in a drastic decrease of the electrochemical signal. However, when the target ssDNA (ssDNA-2) or protein was present, the ssDNA-1 would bind the target, allowing the electron transfer and leading to the increase of peak currents. Muthurasu *et al.* demonstrated a simple strategy to detect and quantify H_2O_2 using electrochemical methods by employing horseradish peroxidase (HRP) functionalized GQDs.[75] CV and CA electrochemical techniques were employed to investigate redox property, electron transfer behaviour and H_2O_2 sensing experiments. This particular electrochemical biosensor showed the sensitivity values of 0.905 and 7.057 µA mM^{-1} and LOD of ~530 and 2.16 µM along with a fast response time of ~2-3 s. Jiang *et al.* fabricated a nonenzymatic H_2O_2 sensor based on AgNPs deposited porous g-C3N4 (Ag/p-g-C$_3$N$_4$) using nitrogen-doped GQDs (N-GQDs) as effective photocatalyst (Fig. 10).[76] The CV and amperometry results showed that the Ag/p-g-C$_3$N$_4$ composite responsed to H_2O_2 with wide linear range and low LOD. Since GQDs exhibited similar peroxidase-like activity, another non-enzymatic H_2O_2 detection in living cells was also realized on a covalently assembled GQDs/Au electrode.[77]
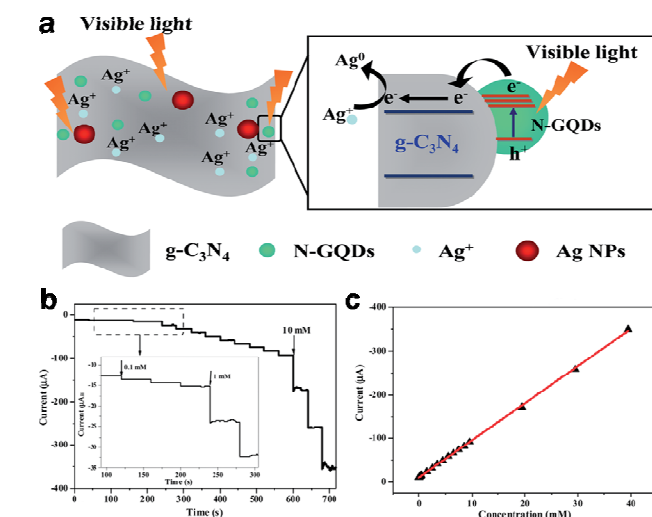

Fig. 10 (a) A schematic diagram illustrating the proposed mechanism for the photochemical synthesis of Ag/p-g-C$_3$N$_4$ nanocomposites. (b) Typical steady-state response of the Ag/p-g-C$_3$N$_4$/GCE to successive injection of H_2O_2 into the stirred N$_2$-saturated 0.2 M PBS at pH 7.4 (applied potential: -0.30 V), and (c) the corresponding calibration curve. Reprinted with permission from ref. 76, copyright 2014 Royal Society of Chemistry.

Razmi *et al.* presented a new, simple and low cost glucose biosensor using glucose oxidase (GOx) and GQDs.[78] They immobilized GOx on the GQDs modified carbon ceramic electrode (CCE) and direct electrochemistry of GOx was realized. The developed biosensor (Gox-GQD/CCE) responded efficiently to glucose presence over the concentration range 5-1270 mM with the LOD of 1.73 mM. The high performance of the biosensor was attributed to the large surface-to-volume ratio, excellent biocompatibility of GQDs, porosity of GQDs/CCE, and the abundance of hydrophilic edges as well as hydrophobic plane in GQDs which enhanced the enzyme absorption on the electrode surface.

Wang *et al.* designed a novel sandwich-type electrochemical immunosensor using Fe$_3$O$_4$@GQDs hybrid and apoferritin-encapsulated Cu (Cu-apoferritin) nanoparticles as labels for highly selective and sensitive detection of avian leukosis virus subgroup J (ALVs-J) (Fig. 11).[79] GQDs were used both for the conjugation of primary ALVs-Jantibodies (Ab1) and immobilization of secondary ALVs-Jantibodies (Ab2) after compounded with Fe$_3$O$_4$. Cu-apoferritin nanoparticles were first selected to immobilize onto Fe$_3$O$_4$@GQDs hybrid as electroactive probes. After the sandwich-type assembly, Cu was released from the apoferritin cavity, and then was detected by DPV. The huge surface area of GQDs increased the loading of antibodies and Cu-apoferritin nanoparticles, and a large amount of electroactive probes could be capsulated into the cavity of apoferritin, which increased the electrochemical signal significantly. Moreover, the proposed immunosensor displayed excellent analytical performance for the detection of ALVs-J ranging from $10^{2.08}$ to $10^{4.50}$ TCID$_{50}$ mL^{-1} with an LOD of 115 TCID$_{50}$ mL^{-1}.
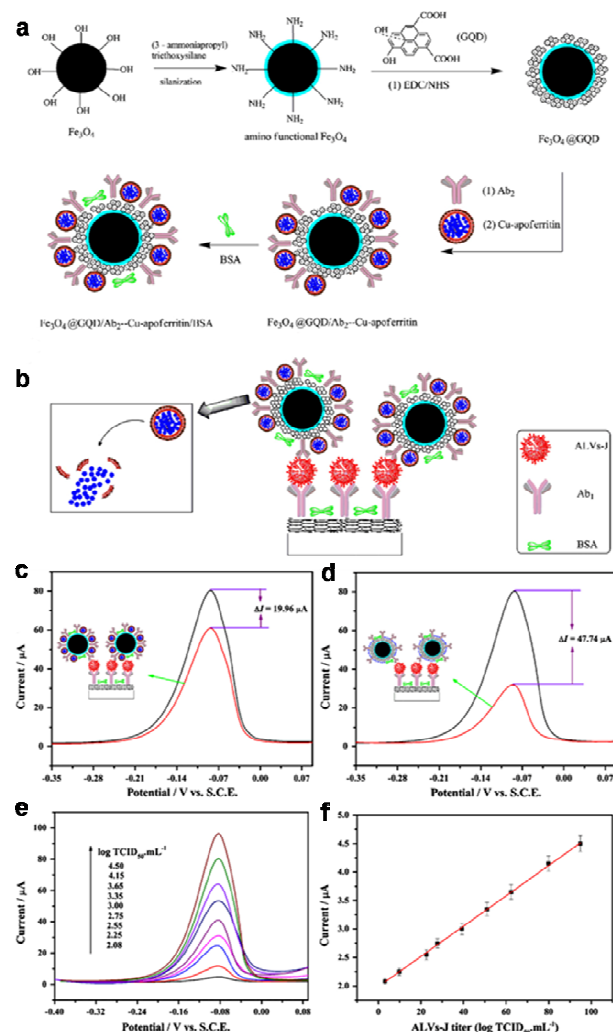

Fig. 11 Schematic representation of the preparation of Fe$_3$O$_4$@GQDs/Ab$_2$-Cu-apoferritin/BSA (a) and immunosensor (b). The DPV comparisons for the proposed immunosensors with (upper curve) and without (lower curve) GQDs (c) and apoferritin (d). (e) DPV responses of the immunosensor with increasing ALVs-J concentrations under the optimized conditions ($10^{2.08}$, $10^{2.25}$, $10^{2.55}$, $10^{2.75}$, $10^{3.00}$, $10^{3.35}$, $10^{3.65}$, $10^{4.15}$,

$10^{4.50}$ TCID$_{50}$ mL^{-1}). (f) Calibration curve. Reprinted with permission from ref. 79, copyright 2013 Elsevier.

3.3 ECL biosensors

ECL, a smart combination of chemiluminescence (CL) and electrochemistry, is a valuable detection method and becoming increasingly recognized in analytical chemistry due to its high sensitivity, simplified set-up, label-free nature and low background signal. A series of semiconductor nanocrystals (such as semiconductor QDs, C-Dots and silicon QDs), have been reported to exhibit ECL emission, which show promise for the construction of ECL biosensors.[80,81] ECL emission was observed from GQDs as well,[30,82-85] and the considerable ECL mechanism of the GQDs was believed to form the excited state GQDs* with the help of the coreactant (such as $S_2O_8^{2-}$, H_2O_2 or TPA)[30,82-84].

Yang *et al.* designed a novel sandwich-type ECL immunesensor by using gold-silver nanocomposite-functionalized graphene (GN-Ag-Au) as sensor platform and GQDs functionalized porous PtPd nanochains (pPtPd) as signal amplifiers for the detection of a tumor marker (Fig. 12).[82] The possible response mechanism for the anodic ECL was proposed in the presence of coreactant TPA. The proposed ECL immunosensor exhibited good precision, acceptable stability and reproducibility. Under optimal conditions, the ECL immunosensors exhibited a wide detection range (0.002-70 U mL^{-1}) and a low LOD (0.96 mU mL^{-1}) for carbohydrate antigen 199 (CA199) in real serum samples.
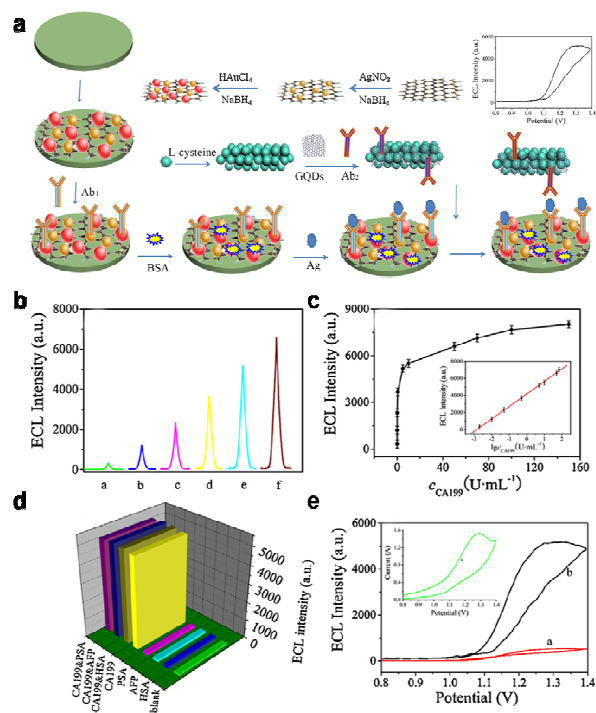

Fig. 12 (a) Schematic illustration of the fabrication procedure of the immunosensor. (b) ECL of the immunosensor at various concentrations of CA199 (a: 0.002, b: 0.01, c: 0.05, d: 0.5, e: 5, f: 50 U mL^{-1}, respectively). (c) Relationship between ECL and the CA199 concentration, each point was the average of ten measurements. (d) The selectivity of the ECL immunosensor. (e) ECL-potential curves of pure GQDs (red curve), pPtPd@GQD (black curve) and cyclic voltammogram (inset) of pPtPd@GQD on the electrode in pH 7.4 PBS containing TPA. Reprinted with permission from ref. 82, copyright 2013 Elsevier.

Using $K_2S_2O_8$ as coreactant, Lu *et al.* constructed an ECL sensor *via* an electrochemiluminescence resonance energy transfer (ERET) between GQDs and gold nanoparticles (AuNPs) for DNA damage detection.[83] The bright blue luminescent GQDs prepared by thermal reduction coupled with UV-light irradiation displayed strong and stable ECL behavior. Au-NPs were linked with a probe of ssDNA (cp53 ssDNA) to form AuNPs-ssDNA. The ECL signal of the GQDs could be quenched by non-covalent binding of the AuNPs-ssDNA to the GQDs, due to the occurrence of an ERET between GQDs and AuNPs. When AuNPs-ssDNA was then hybridized with target p53 DNA to form AuNPs-dsDNA, the non-covalent interaction between GQDs and ds-DNA weakened and the ECL of the GQDs recovered. Therefore, the difference between the quenching efficiencies of AuNPs-ssDNA and AuNPs-dsDNA to GQDs engendered an ECL sensor for detection of target p53 ssDNA with an LOD of 13 nM. In addition, the resultant ECL sensor could also be used for DNA damage detection based on the different bonding abilities of damaged target p53 ssDNA and cp53 ssDNA linked AuNPs.

By combining intense ECL of GQDs and aptamer technique, Lu *et al.* proposed a novel ECL aptamer sensor for measuring ATP.[84] A newly anodic ECL was observed from the water-soluble GQDs with H_2O_2 as coreactant, and the ECL induced a strong light emission at a low potential. As an amplified element, GQDs doped SiO$_2$ nanospheres (SiO$_2$/GQDs) were used to produce an amplified ECL signal and improved the sensitivity of the sensor. The proposed ECL aptamer sensor exhibited excellent analytical performance for ATP determination, ranging from 5.0×10^{-12} to 5.0×10^{-9} mol L^{-1} with the LOD of 1.5×10^{-12} mol L^{-1}.

In addition, Dong *et al.* presented an ECL sensor for the detection of H_2O_2 using hydrazide-modified single-layer GQDs (HM-SGQDs) (Fig. 13).[85] Due to the introduction of hydrazine groups and the formation of abundant luminol-like units, HM-SGQDs exhibited unique PL, CL and anodic ECL properties. The hydrazide groups of HM-SGQDs could be electrochemically oxidized in alkaline solutions, producing a strong anodic ECL signal. The ECL intensity could be enhanced sensitively by H_2O_2, and the enhanced ECL intensity was proportional to the concentration of H_2O_2 in a wide range of 3 to 500 mM with an LOD of 0.7 mM.
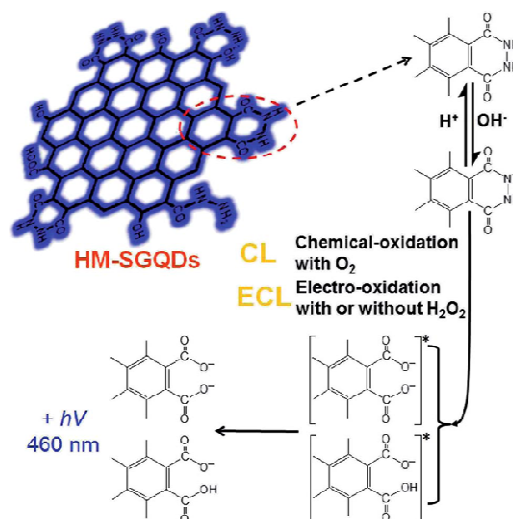
Fig. 13 CL and ECL mechanisms of HM-SGQDs. Reprinted with permission from ref. 85, copyright 2014 Royal Society of Chemistry.

4. Bioimaging

Fluorescent organic dyes and semiconductor QDs have been widely used for bioimaging or visualization of living cells.[86-89] However, photobleaching of organic dyes and toxicity of heavy metal contained in semiconductor materials prompt us to find better substitutes. GQDs, which exhibit stable PL, low toxicity and good biocompatibility, provide a much better choice for both *in vitro* and *in vivo* bioimaging.

4.1 *In vitro* imaging

4.1.1 Stem cells imaging

Stem cells are central to the understanding of native development and tissue regeneration, which give rise to tissue progenitor cells and in turn differentiate into tissue-forming cells.[90-92] Because of the particularity of stem cells, their labeling poses a considerable challenge.[93] Bright yellow fluorescent GQDs prepared by our group[33] have demonstrated direct and easy penetration into stem cells without affecting their viability, proliferation or differentiation capacity. This is the first use of stabilizer-free graphene as a fluorescent labelling agent in long term stem cell imaging. Three different kinds of stem cells, neurospheres cells (NSCs), pancreas progenitor cells (PPCs) and cardiac progenitor cells (CPCs) were incubated with GQDs at a concentration of 25 mg mL^{-1} for 24 h at 37 ºC. As shown in the confocal fluorescent images (Fig. 14), the morphology of stem cells could be clearly discerned with the internalized GQDs. The confocal section images indicated that GQDs easily entered into the cytoplasmic areas of the stem cells. methylthiazolyldiphenyl-tetrazolium bromide (MTT) assay demonstrated low cytotoxicity of GQDs for the stem cell imaging. However, the fluorescent C$_{60}$ nanoparticles which could easily penetrate into human lung carcinoma (A549) and human breast cells (MCF-7) were not detected inside stem cells.[94] And the stem cells died immediately when cultured with 5 nm CdS nanoparticle without surface modification owing to the cytotoxicity of Cd^{2+}. Therefore, such GQDs have a distinct advantage in terms of their biocompatibility and their penetrating power to stem cells without further bioconjugation.
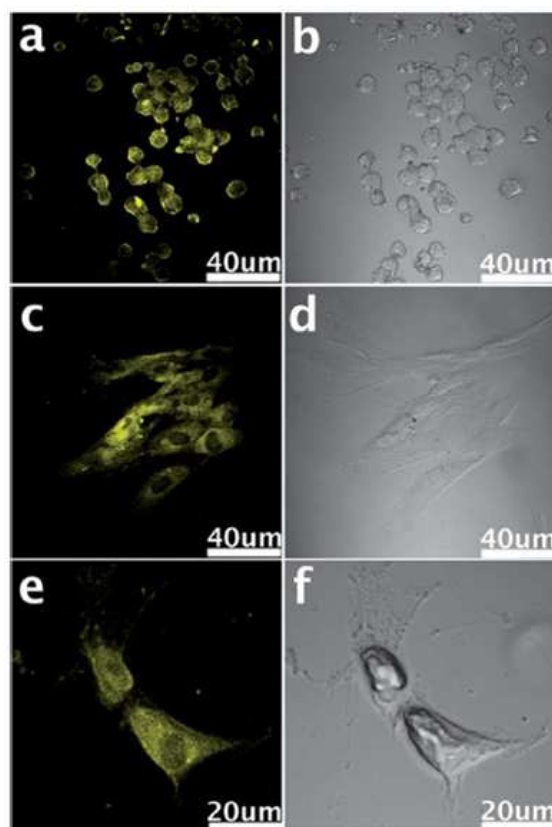

Fig. 14 Confocal fluorescence microscopy images of stem cells of NSCs (a), PPCs (c) and CPCs (e) with the fluorescent GQDs incorporated at the excitation wavelength of 405 nm and corresponding images under bright field (b, d, f). Reprinted with permission from ref. 33, copyright 2012 Royal Society of Chemistry.

We further investigated the uptake mechanism and biocompatibility of such GQDs with human neural stem cells (hNSCs).[95] TEM images (Fig. 15) confirmed the GQDs were indeed internalized by hNSCs *via* the endocytosis mechanism and were located in the cytoplasm. We found that GQDs did not affect the self-renewal capacity of hNSCs. Single cell dissociated from GQDs-labeled hNSCs finally formed large neurospheres, and the cells expressing the cell type-specific marker for hNSCs, nestin, were identified. Furthermore, no significant change was found in the viability, proliferation, metabolic activity of NSCs after treatment with GQDs, and GQDs did not affect the differentiation potential of hNSCs. After 14 days of differentiation, no difference was detected in the hNSC growth between the control group and the 25 μg mL^{-1} GQDs treatment group (Fig. 16a, b). Cells from both groups showed elongated cell shapes with neurite outgrowths, resulting in the formation of an interconnected neuronal network. Then glial fibrillary acidic protein (GFAP) and neuron-specific class III beta-tubulin (tubulin βIII) were examined using immunocytochemistry, and hNSCs could spontaneously differentiate into neurons and glial cells (Fig. 16c-f). The above results open a promising avenue for labeling stem cells with GQDs and also offer a potential opportunity to develop GQDs for biomedical applications.
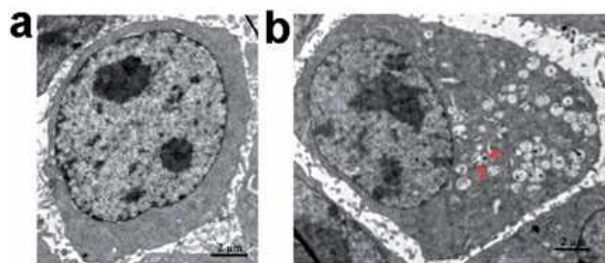
Fig. 15 TEM images of hNSCs after 24 h incubation with 25 μg mL⁻¹ of GQDs. (a) Control and (b) GQDs. Red arrows in (b) indicate intrracellular vesicles engulfing GQDs. Reprinted with permission from 5 ref. 95, copyright 2014 Royal Society of Chemistry.
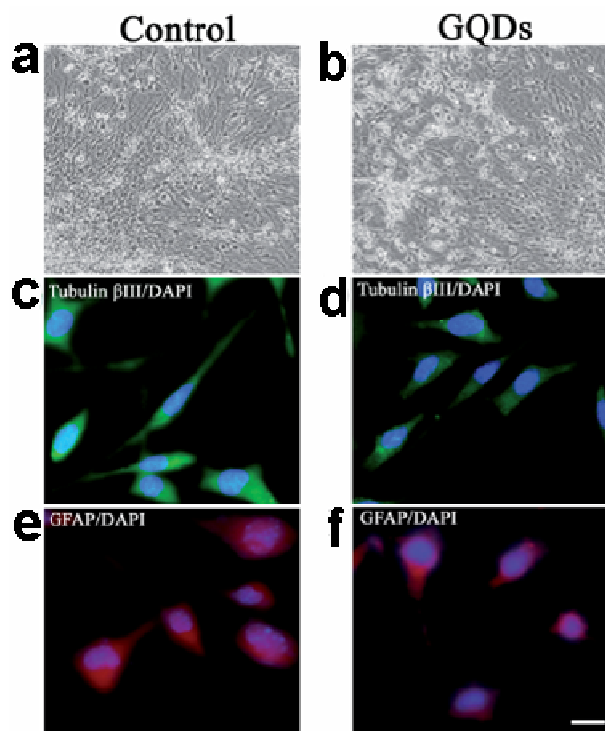

Fig. 16 Bright-field images of the hNSCs differentiated for 14 days (a: control; b: 25 μg mL⁻¹ GQDs). Representative microphotographs demonstrated tubulin βIII⁺ (green, c and d) and GFAP⁺ (red, e and f) cells. 10 The nuclei were counterstained with DAPI (blue). Scale bar: 20 μm. Reprinted with permission from ref. 95, copyright 2014 Royal Society of Chemistry.

4.1.2 Tumor cells imaging

Besides stem cells bioimaging, most GQDs-based biomarkers 15 focus on tumor cells. Various studies proved that fluorescent GQDs could enter tumor cells easily. Our group recently reported B-GQDs for imaging of Hela cells (Fig. 17a, b).[19] Zhu *et al.* cultured human osteosarcoma (MG-63) cells with solvothermally prepared GQDs and showed the two-color imaging by using 20 different excitaion wavelength (Fig. 17c, d).[54]
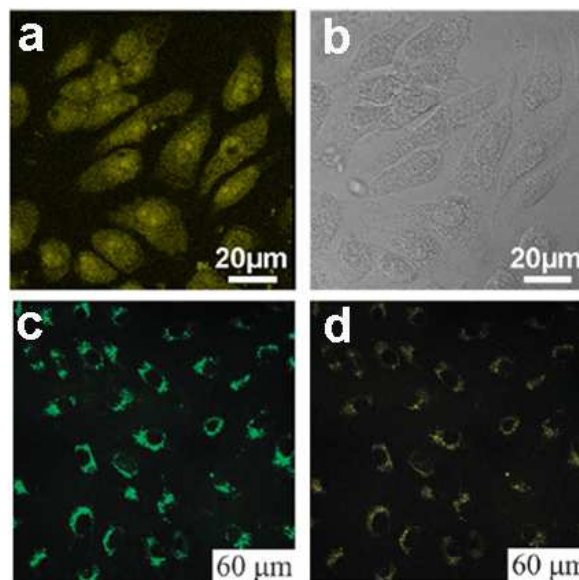

Fig. 17 (a) Confocal fluorescence microscopy images of Hela cells with B-GQDs coated with liposomes at the excitation wavelength of 405 nm and corresponding image under bright field (b). (c), (d) are washed MG-25 63 cells imaged under bright field, 405 nm, 488 nm excitations, respectively. Reprinted with permission from: (a) and (b): ref. 19, copyright 2014 Elsevier, (c) and (d): ref. 54, copyright 2011 Royal Society of Chemistry.

Peng *et al.* chose the green luminescent GQDs to incubate with 30 human breast cancer cell lines T47D with the nucles stained with DAPI,[24] The obtained images (Fig. 18a, b) clearly visualized the phase contrast image of T47D cells, nucleus stained blue with DAPI, agglomerated high contrast fluorescent image of green GQDs around each nucleus and overlay image of cell with phase 35 contrast, DAPI and green GQDs. Dong *et al.* incubated human breast cancer MCF-7 cells with GQDs prepared by acidic oxidation,[23] and bright green color could be observed when imaged on the confocal laser scanning microscope with excitation at 488 nm (Fig. 18c). The section analysis of one MCF-7 cell 40 indicated that GQDs were able to label not only the cell membrane and the cytoplasm, but also the nucleus (Fig. 18d). That was the first time for luminescent carbon nanomaterials to label the cell nucleus. In addition, Hela cells,[96-100] A-549 cells,[101,102] macrophages and hepatocellular cells[103,104] were also 45 adopted to incubate with fluorescent GQDs by several groups. All these studies suggested the low cytotoxicity and excellent biocompatibility of GQDs by MTT assay, thus they could be used as an eco-friendly material in biolabeling.
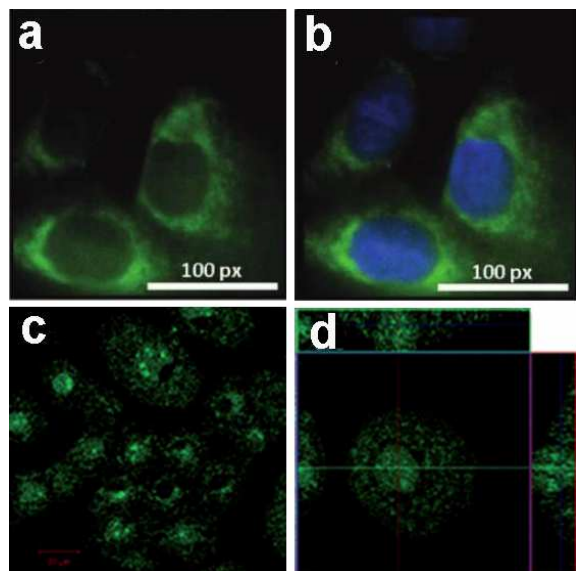
RSC Advances Accepted Manuscript

Fig. 18 Fluorescent images of human breast cancer cell T47D after incubation with green GQDs for 4 h (a) agglomerated green GQDs surrounding each nucleus. (b) The overlay high contrast image of nucleolus stained with blue DAPI and GQDs (green) staining. (c) Images of human breast cancer MCF-7 cells labeled with GQDs taken by a confocal laser scanning microscope (CLSM): (c) fluorescent image; (d) section analysis. Reprinted with permission from: (a) and (b): ref. 24, copyright 2012 American Chemical Society, (c) and (d): ref. 23, copyright 2012 Royal Society of Chemistry.

4.1.3 Targeted cellular imaging

It is a well known fact that chemotherapy exhibits massive side effects due to the indiscriminate distribution of anticancer drugs to cancerous and healthy cells.[105,106] Targeted cancer cellular imaging, as a fundamental research, promotes cancer detection and targeted therapeutic modalities for effective cancer chemotherapy with improved safety. Since GQDs can be modified or linked with special bioactive species, targeted cellular bioimaging based on GQDs has also been developed.

In an early study, Sun *et al.* realized selective targeted cellular imaging by conjugating a B-cell specific antibody Rituxan (anti-CD20) to the PEGylated nanosized graphene oxide (NGO-PEG). After incubating B-cells and T-cells with NGO-PEG-Rituxan, the intrinsic near-infrared (NIR) PL of NGO-PEG was detected selectively on positive Raji B-cell surfaces and not on negative CEM T-cells (Fig. 19a, b). Then a widely used cancer drug doxorubicin (DOX) was loaded onto NGO-PEG-Rituxan for selective killing of cancer cells *in vitro*.[107]
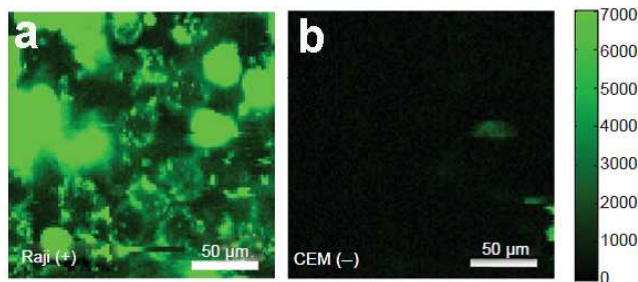

Fig. 19 NIR fluorescence images of CD20 positive Raji B-cells (a) and CD20 negative CEM B-cells (b) treated with NGO-PEG-Rituxan conjugate. The scale bar shows the intensity of total NIR emission (in the range 1100-2200 nm). Reprinted with permission from ref. 107, copyright 2008 Springer.

Nigam *et al.* reported GQDs conjugated with hyaluronic acid functionalized human serum albumin nanoparticles (HA-HSA-NPs) for pancreatic cancer specific bioimaging.[108] Panc-1 cell lines were rich in CD-44, which was a receptor for hyaluronic acid and responsible for chemotherapy-resistant pancreatic cancer cells. After incubated with GQDs tagged HA-HSA-NPs, strong green fluorescence was observed inside the pancreatic cells resulting from the efficient uptake of HA-HSA-NPs while unfunctionalized HSA-NPs exhibited weak fluorescence signals (Fig. 20), indicating that HA-HSA-NPs could efficiently target CD-44 by expressing pancreatic cells *via* HA-mediated endocytosis pathways.
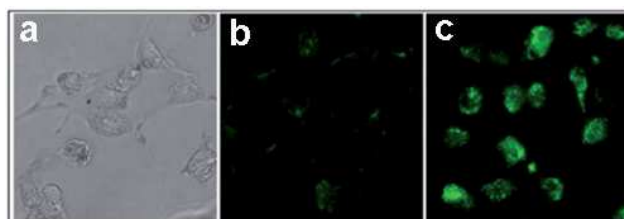

Fig. 20 Fluorescence imaging of Panc-1 cells after 24 h incubation in the presence of GQD-conjugated HSA nanoparticles in Dulbecco's modified Eagle's (DMEM) media with 10% fetal bovine serum in CO_2 incubator at 37 °C; (a) cells without staining (control); (b) HSA nanoparticles with GQDs only; (c) HSA NPs functionalized with HA and GQDs. Reprinted with permission from ref. 108, copyright 2014 Royal Society of Chemistry.

In a more recent study, fluorescent GQDs were prepared and conjugated with folic acid (FA) to demonstrate highly selective and specific tumour cell imaging by Wang *et al.*[109] The fluorescence of the GQDs in FA overexpressed HeLa cells was considerably stronger than that in the A549 and HEK293A cells (Fig. 21), which expressed FA receptor (FR) at a low level, indicating that GQD-FA was internalized *via* FR-induced endocytosis. The FA-conjugated GQDs were then employed as a carrier of the antitumor drug DOX for targeted cell delivery.
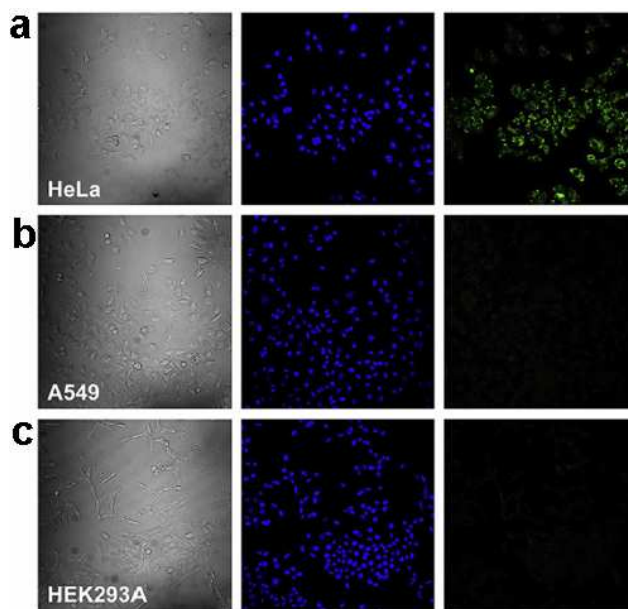

Fig. 21 Confocal laser scanning microscopy of (a) HeLa human cervical carcinoma cells, (b) A549 adenocarcinomic human alveolar basal epithelial cells, and (c) HEK293A normal human embryonic kidney cells

incubated with GQD-FA (20.0 μg mL^{-1}) at 37 ºC for 10 min. Left column: bright field images. Middle column: fluorescence image with Hoechst nuclear stained (blue). Right column: GQD fluorescence image (green). Reprinted with permission from ref. 109, copyright 2014 Elsevier.

5 Insulin-conjugated GQDs were synthesized and utilized for specific labeling and dynamic tracking of insulin receptors in 3T3-L1 adipocytes by Zheng *et al.*[110] They investigated the dynamic trafficking of insulin receptors using total internal reflection fluorescence microscopy (TIRFM), which evanescently 10 and selectively illuminated the thin plasmalemmal region. After preincubating adipocytes with insulin-GQDs to allow endocytosis and exocytosis of insulin receptors, time-lapse images were taken under total TIRFM (Fig. 22). It demonstrated that GQDs could be readily conjugated with a wide range of 15 biomolecules without interfering with their activities and then used to specifically label and track molecular targets involved in dynamic cellular process in live cells.
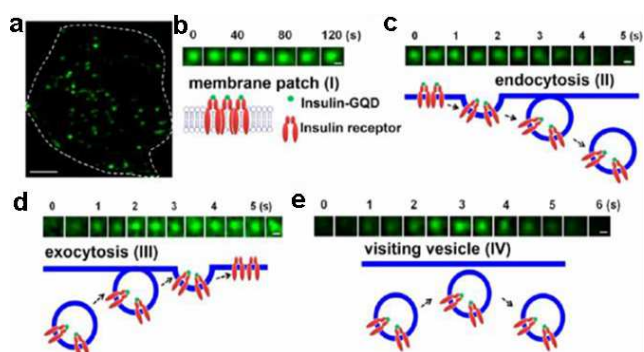

Fig. 22 Tracking the dynamics of insulin receptors in living adipocytes 20 using TIRFM. (a) Typical TIRFM image of a 3T3-L1 adipocyte after 1 h incubation of insulin-GQDs. Scale bar = 5 μm. (b) Membrane patch consisting of insulin-GQD/insulin receptor clusters (type I). (c) Endocytosis of fluorescent membrane patches into a vesicle (type II). (d) Exocytosis of a vesicle containing insulin-GQD/insulin receptor 25 complexes (type III). (e) Transient approaching and retrieval of insulin-GQD/insulin receptor containing vesicle (type IV). Scale bars = 0.2 μm. Reprinted with permission from ref. 110, copyright 2013 American Chemical Society.

4.1.4 Two-photon imaging

30 With advantages of a larger penetration depth, a minimized tissue auto fluorescence background, the avoidance of harmful UV or blue excitations and the reduction of photo damage in biotissues, two-photon imaging has received a great deal of attention in biological research. Li *et al.* found strong PL in graphene oxide 35 nanoparticles (GONs) from two-photon excitation by an ultrafast pulsed laser. The GONs were suitable for two-photon luminescence imaging (Fig. 23a, b).[111] Liu *et al.* reported N-GQDs as efficient two-photon fluorescence probes for cellular and deep-tissue imaging.[18] The GQDs-stained Hela cells became 40 brightly illuminated when imaged under the microscope with excitation at 800 nm (Fig. 23c, d). The two-photon absorption cross-section of N-GQDs reached 48 000 Göppert-Mayer units, which far surpassed that of the organic dyes and was comparable to that of the high performance semiconductor QDs.
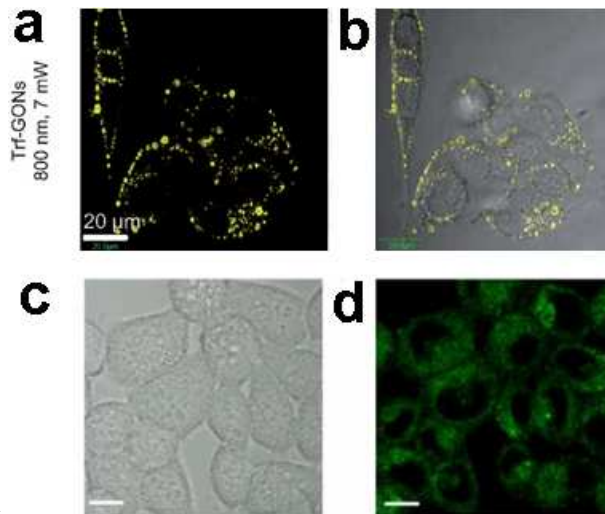

45 **Fig. 23** *In vitro* two-photon luminescence of GONs (a, b). Two-photo cell imaging under (c) bright field and (d) 800 nm excitation. (All scale bars: 10 μm.) Reprinted with permission from: (a) and (b): ref. 111, copyright 2012 Wiley-VCH, (c) and (d): ref. 18, copyright 2013 50 American Chemical Society.

4.2 *In vivo* imaging

Since Yang *et al.* firstly explored the feasibility of C-Dots as a fluorescence contrast agent in mice,[112] a variety of C-Dots have been synthesized and used for *in vivo* imaging. [113-115] GQDs, 55 similar to C-Dots, can also be applied for *in vivo* imaging. PEGylated nanographene sheet (NGS-PEG) with an average size of 30 nm prepared by Yang *et al.* was administered into the mice after labeling with a commonly used NIR fluorescent dye Cy7. *In vivo* fluorescence imaging revealed high tumor uptake of NGS in 60 several xenograft tumor mouse models (Fig. 24). Then the strong optical absorbance of NGS in the NIR region was utilized for *in vivo* photothermal therapy.[116]
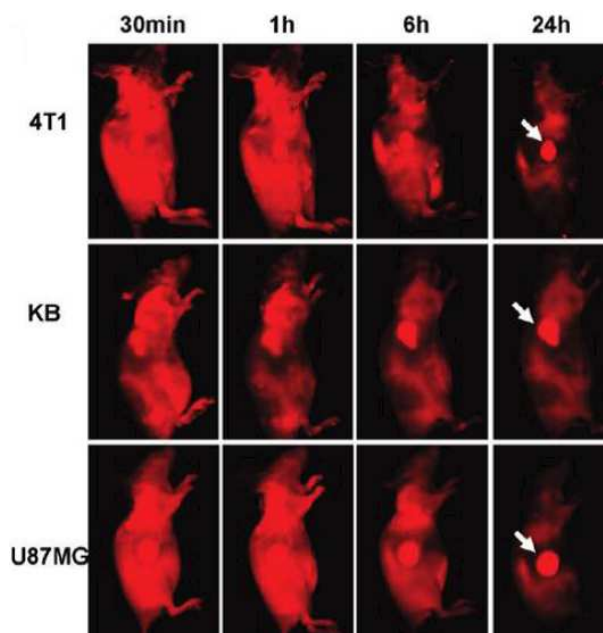

Fig. 24 Spectrally unmixed in vivo fluorescence images of 4T1 tumor 65 bearing Balb/c mice, KB, and U87MG tumor bearing nude mice at different time points post injection of NGS-PEG-Cy7. Reprinted with permission from: ref. 116, copyright 2010 American Chemical Society.

The feasibility of GQDs prepared by a one-step pyrolysis of L-glutamic acid for *in vivo* bioimaging was investigated in mice by Wu *et al.*[44] After injecting GQDs subcutaneously into the back of nude mice and intramuscularly into the right back leg, the fluorescence images of the mice under different excitation and emission filters were obtained (Fig. 25). The detectable fluorescence region extended with the longer excitation and emission wavelengths from the intramuscular injection spot of the right back leg, demonstrating that longer wavelengths for *in vivo* fluorescence imaging had better penetration ability than the short ones.

Ge *et al.* investigated the *in vivo* fluorescence imaging capability of red fluorescent GQDs prepared *via* a hydrothermal method with polythiophene derivatives.[41] After the injection of GQDs aqueous solution into the back of a nude mouse, the injection sites showed much higher fluorescence intensity than the background signal produced by the mouse skin as depicted in Fig. 26a, b. Furthermore, no apparent fluorescence intensity decay was observed at the injection sites, and the injected GQDs did not show evidence of obvious diffusion even 1 week after injection. More importantly, GQDs could be applied as a photodynamic therapy (PDT) agent for the simultaneous imaging and highly efficient treatment of cancer. Using female BALB/nu mice with subcutaneous breast cancer xenografts as an animal model, three groups, the PDT group, the control groups included mice that received a GQDs injection at the same dose but were not irradiated (the C1 group) and mice that did not received a GQDs injection but were irradiated (the C2 group) were chosen to evaluate the performance of the GQDs for *in vivo* PDT. In the PDT group, the tumours first turned dark and festered, which increased the tumour size slightly (Fig. 26c). The tumours began to decompose after 9 days and were destroyed after 17 days, leaving black scars at the original sites, which fell off ~1 week later. No tumour regrowth was observed in the PDT group over the course of 50 days. In contrast, the tumours in the C1 and C2 groups grew significantly during the study period (Fig. 26d), indicating that neither light irradiation nor GQDs injection alone inhibited the tumor growth.
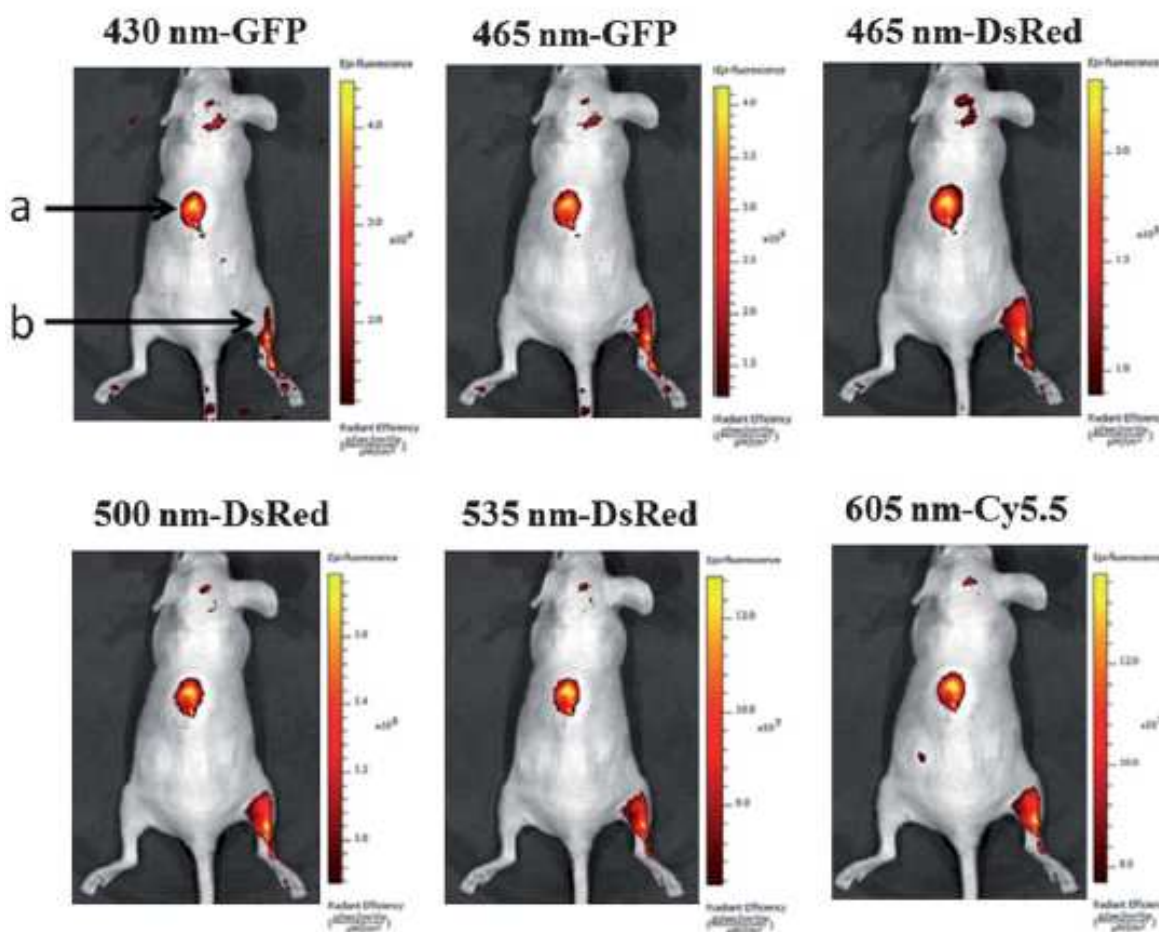
Fig. 25 *In vivo* fluorescence imaging of mice injected GQDs subcutaneously (spot a) and intramuscularly (spot b). The images were taken at various excitation wavelengths and emission wavelengths indicated at the top of each image. A 100 mL aliquot of 25 mg mL^{-1} GQDs was injected into each spot. The following emission bandpass filters were used: GFP: 515-575 nm; DsRed: 575-650 nm; Cy5.5: 695-770 nm. Reprinted with permission from ref. 44, copyright 2013 Royal Society of Chemistry.

Fig. 26 *In vivo* imaging and PDT. (a) Bright-field image and (b) red-fluorescence image after subcutaneous injection of GQDs in different areas. The excitation wavelength was 502-540 nm, and the collected fluorescence channel was 695-775 nm. (c) Photographs of mic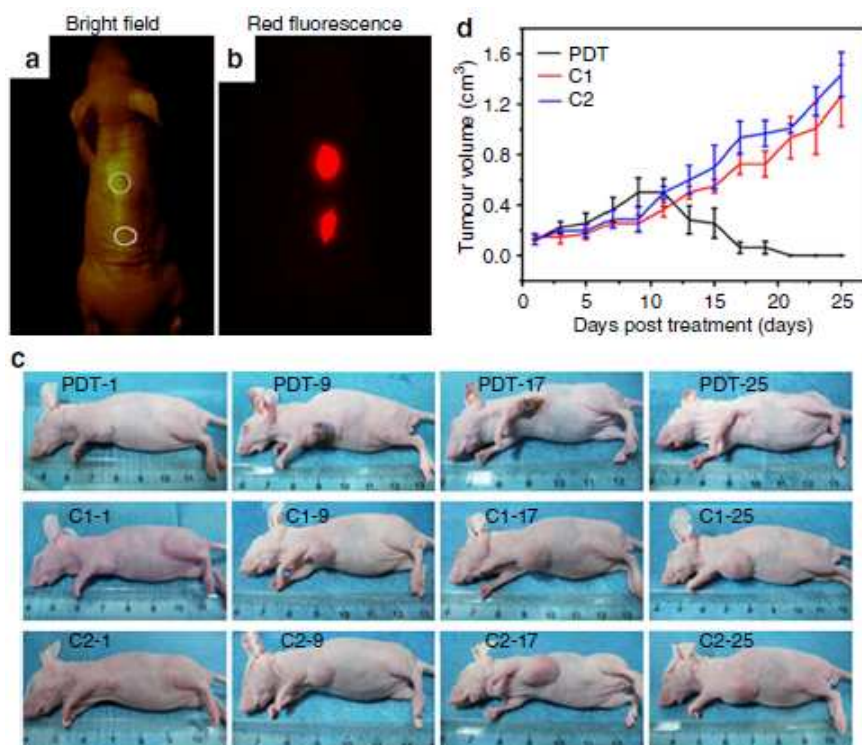e after various treatmentsion the 1st, 9 th, 17 th and 25 th day. (PDT: GQDs + light irradiation; C1: GQDs only; C2: light irradiation only) (d) Time-dependent tumour growth curves (n=5) after different treatments. *P* < 0.05 for each group. Reprinted with permission from ref. 41, copyright 2014 Nature Publishing Group.

5. Conclusions and future perspectives

In this review, GQDs have been comprehensively introduced from the aspects of synthetic approaches, structure, PL properties and applications for biosensing and bioimaging. We have discussed GQDs-based PL, electrochemical and ECL biosensors with high sensitivity and selectivity for the detection of ions, biomolecules and small organic molecules with aromatic structures. In addition, GQDs are suitable materials for both *in vitro* and *in vivo* bioimaging. The use of GQDs for biosensing and bioimaging has achieved great success within a short time.[117-118] However, GQDs have yet to be exploited because of a number of current problems such as short wavelength emission, low yield and QY.[119] Meanwhile, strong two/three-photon fluorescent GQDs for live deep-tissue imaging and special biomolecule modified GQDs for targeted cancer imaging, diagnosis and therapy are particularly desired. Herein, we speculate the future perspectives on GQDs-based biosensors and biomarkers as follows.

5.1 QY improvement

The highest QY of GQDs reported so far is 54.5% with blue fluorescence emission,[44] but the QY of GQDs with other color fluorescence emission is less than 20%, much lower than traditional semiconductor QDs and organic dyes. Therefore the QY improvement in longer wavelength emission of GQDs is challenging. With the achievement of uniform size, shape and edge, the multicolor PL and high QY of GQDs will be more promising for biosensing and bioimaging.

5.2 Red/near-IR and the second near-IR (NIR-II) PL emission GQDs for bioimaging

Due to the auto-fluorescence and light scattering background of biological specimens in the short-wavelength region, fluorescent materials emitting in the long-wavelength region are expected to provide a deeper light penetration into the specimens with a higher imaging contrast. Biological imaging with fluorescent agents in the long NIR region (1000-1700 nm, terrned the second near-IR region), which has received growing interests in recent years, can afford even deeper penetration than the traditional NIR (750-900 nm) imaging techniques.[120-124] GQDs with bright fluorescence emissions emphasized in the red/near-IR as well as the NIR-II spectral regions are desired for effective tissue penetration and *in vivo* imaging,

5.3 Biosensing and bioimaging based on the upconversion PL of GQDs

Upconversion PL of GQDs provides the advantage in exciting near-IR light using multi-photon excitation. It has received a great deal of attention for its promising applications in both basic biological researches and clinical diagnostics with the avoidance of harmful UV or blue excitations and the reduction of photo damage in biotissues. Therefore, upconversion PL will expand the applications of GQDs for biosensing and bioimaging.

5.4 GQDs functionalization for specific labeling

Researches on potential applications of GQDs as a cell imaging agent mainly concentrate on the uptake of bare GQDs by cells without considering the selectivity and function of the agent. Functional groups on the GQDs can be modified or conjugated with a wide range of biomolecules, thus contributing to specifically label and track molecular targets. It is of great significance for the exploitation of surface functionalization in GQDs for controlled coupling with bioactive species to enable specific targeting in cellular, *in vivo* imaging, noninvasively detecting disease of living biosystems and related biomedical applications.

Acknowledgements

Notes and references

1. C. Chung, Y. K. Kim, D. Shin, S. R. Ryoo, B. H. Hong and D. H. Min, *Acc. Chem. Res.*, 2013, **46**, 2211-2224.
2. V. Georgakilas, M. Otyepka, A. B. Bourlinos, V. Chandra, N. Kim, K. C. Kemp, P. Hobza, R. Zboril and K. S. Kim, *Chem. Rev.*, 2012, **112**, 6156-6214.
3. K. S. Novoselov, A. K. Geim, S. V. Morozov, D. Jiang, Y. Zhang, S. V. Dubonos, I. V. Grigorieva and A. A. Firsov, *Science*, 2004, **306**, 666-669.
4. K. S. Novoselov, Z. Jiang, Y. Zhang, S. V. Morozov, H. L. Stormer, U. Zeitler, J. C. Maan, G. S. Boebinger, P. Kim and A. K. Geim, *Science*, 2007, **315**, 1379-1379.
5. S. Fujii and T. Enoki, *J. Am. Chem. Soc.*, 2010, **132**, 10034-10041.
6. K. A. Ritter and J. W. Lyding, *Nat. Mater.*, 2009, **8**, 235-242.
7. X. Li, X. Wang, L. Zhang, S. Lee and H. Dai, *Science*, 2008, **319**, 1229-1232.
8. L. A. Ponomarenko, F. Schedin, M. I. Katsnelson, R. Yang, E. W. Hill, K. S. Novoselov and A. K. Geim, *Science*, 2008, **320**, 356-358.
9. J. H. Shen, Y. H. Zhu, X. L. Yang and C. Z. Li, *Chem. Commun.*, 2012, **48**, 3686-3699.
10. S. J. Zhu, S. J. Tang, J. H. Zhang and B. Yang, *Chem. Commun.*, 2012, **48**, 4527-4539.
11. Y.-P. Sun, B. Zhou, Y. Lin, W. Wang, K. A. S. Fermando, P. Pathak, M. J. Meziani, B. A. Harruff, X. Wang, H. Wang, P. G. Luo, H. Yang, M. E. Kose, B. Chen, L. M. Veca and S.-Y. Xie, *J. Am. Chem. Soc.,* 2006, **128**, 7756-7757.
12. Y. Li, Y. Hu, Y. Zhao, G. Shi, L. Deng, Y. Hou and L. Qu, *Adv. Mater.,* 2011, **23**, 776-780.
13. S. Zhu, Q. Meng, L. Wang, J. Zhang, Y. Song, H. Jin, K. Zhang, H. Sun, H. Wang and B. Yang, *Angew. Chem., Int. Ed.,* 2013, **52**, 3953-3957.
14. S. N. Baker and G. A. Baker, *Angew. Chem., Int. Ed.,* 2010, **49**, 6726-6744.
15. X. Zhou, Y. Zhang, C. Wang, X. Wu, Y. Yang, B. Zheng, H. Wu, S. Guo and J. Zhang, *ACS Nano*, 2012, **6**, 6592-6599.
16. R. Liu, D. Wu, X. Feng and K. Muellen, *J. Am. Chem. Soc.*, 2011, **133**, 15221-15223.
17. D. Y. Pan, J. C. Zhang, Z. Li and M. H. Wu, *Adv. Mater.,* 2010, **22**, 734-738.
18. Q. Liu, B. D. Guo, Z. Y. Rao, B. H. Zhang and J. R. Gong, *Nano Lett.*, 2013, **13**, 2436-2441.
19. Z. T. Fan, Y. C. Li, X. H. Li, L. Z. Fan, S. X. Zhou, D. C. Fang and S. H. Yang, *Carbon*, 2014, **70**, 149-156.
20. S. H. Li, Y. C. Li, J. Cao, J. Zhu, L. Z. Fan and X. H. Li, *Anal. Chem.,* 2014, **86**, 10201-10207.
21. H. Sun, L. Wu, W. Wei and X. Qu, *Mater. Today*, 2013, **16**, 433-442.
22. Y. B. Song, S. J. Zhu and B. Yang, *RSC Adv.*, 2014, **4**, 27184-27200.
23. Y. Dong, C. Chen, X. Zheng, L. Gao, Z. Cui, H. Yang, C. Guo, Y. Chi and C. M. Li, *J. Mater. Chem.*, 2012, **22**, 8764-8766.
24. J. Peng, W. Gao, B. K. Gupta, Z. Liu, R. Romero-Aburto, L. Ge, L. Song, L. B. Alemany, X. Zhan, G. Gao, S. A. Vithayathil, B. A. Kaipparettu, A. A. Marti, T. Hayashi, J. J. Zhu and P. M. Ajayan, *Nano Lett.*, 2012, **12**, 844-849.
25. R. Ye, C. Xiang, J. Lin, Z. Peng, K. Huang, Z. Yan, N. P. Cook, E. L. G. Samuel, C. C. Hwang, G. Ruan, G. Ceriotti, A.-R. O. Raji, A. A. Marti and J. M. Tour, *Nat. Commun.*, 2013, **4**, 2943-2948.
26. D. Pan, L. Guo, J. Zhang, C. Xi, Q. Xue, H. Huang, J. Li, Z. Zhang, W. Yu, Z. Chen, Z. Li and M. Wu, *J. Mater. Chem.*, 2012, **22**, 3314-3318
27. Q. Liu, B. D. Guo, Z. Y. Rao, B. H. Zhang and J. R. Gong, *Nano Lett.*, 2013, **13**, 2436-2441.
28. H. Tetsuka, R. Asahi, A. Nagoya, K. Okamoto, I. Tajima, R. Ohta and A. Okamoto, *Adv. Mater.*, 2012, **24**, 5333-5338.
29. S. Chen, J. W. Liu, M. L. Chen, X. W. Chen and J. H. Wang, *Chem. Commun.*, 2012, **48**, 7637-7639.
30. L. L. Li, J. Ji, R. Fei, C. Z. Wang, Q. Lu, J. R. Zhang, L. P. Jiang and J. J. Zhu, *Adv. Funct. Mater.*, 2012, **22**, 2971-2979.
31. S. Zhuo, M. Shao and S. T. Lee, *ACS Nano*, 2012, **6**, 1059-1064.
32. Y. Li, Y. Zhao, H. H. Cheng, Y. Hu, G. Q. Shi, L. M. Dai and L. T. Qu, *J. Am. Chem. Soc.*, 2012, **134**, 15-18.
33. M. Zhang, L. Bai, W. Shang, W. Xie, H. Ma, Y. Fu, D. Fang, H. Sun, L. Fan, M. Han, C. Liu and S. Yang, *J. Mater. Chem.*, 2012, **22**, 7461-7467.
34. D. B. Shinde and V. K. Pillai, *Chem. Eur. J.*, 2012, **18**, 12522-12528.
35. A. Ananthanarayanan, X. Wang, P. Routh, B. Sana, S. Lim, D. H. Kim, K. H. Lim, J. Li and P. Chen, *Adv. Funct. Mater.*, 2014, **24**, 3021-3026.
36. F. Liu, M. H. Jang, H. D. Ha, J. H. Kim, Y.-H. Cho and T. S. Seo, *Adv. Mater.*, 2013, **25**, 3657-3662.
37. L. Lin and S. Zhang, *Chem. Commun.*, 2012, **48**, 10177-10179.
38. Q. Li, S. Zhang, L. Dai and L. Li, *J. Am. Chem. Soc.*, 2012, **134**, 18932-18935.
39. X. Yan, X. Cui and L. Li, *J. Am. Chem. Soc.*, 2010, **132**, 5944-5945.
40. L. Wang, Y. Wang, T. Xu, H. Liao, C. Yao, Y. Liu, Z. Li, Z. Chen, D. Pan, L. Sun and M. Wu, *Nat. Commun.,* 2014, **5**, 5357-5365.
41. J. Ge, M. Lan, B. Zhou, W. Liu, L. Guo, H. Wang, Q. Jia, G. Niu, X. Huang, H. Zhou, X. Meng, P. Wang, C. S. Lee, W. Zhang and X. Han, *Nat. Commun.,* 2014, **5**, 4596-4603.
42. Y. Q. Dong, J. W. Shao, C. Q. Chen, H. Li, R. X. Wang, Y. W. Chi, X. M. Lin and G. N. Chen, *Carbon*, 2012, **50**, 4738-4743.
43. L. Tang, R. Ji, X. Cao, J. Lin, H. Jiang, X. Li, K. S. Teng, C. M. Luk, S. Zeng, J. Hao and S. P. Lau, *Acs Nano*, 2012, **6**, 5102-5110.
44. X. Wu, F. Tian, W. Wang, J. Chen, M. Wu and J. X. Zhao, *J. Mater. Chem. C*, 2013, **1**, 4676-4684.
45. Z. Huang, Y. Shen, Y. Li, W. Zheng, Y. Xue, C. Qin, B. Zhang, J. Hao and W. Feng, *Nanoscale*, 2014, **6**, 13043-13052.
46. J. Lu, P. S. E. Yeo, C. K. Gan, P. Wu and K. P. Loh, *Nat. Nanotechnol.*, 2011, **6**, 247-252.
47. S. J. Zhu, J. H. Zhang, S. J. Tang, C. Y. Qiao, L. Wang, H. Y. Wang, X. Liu, B. Li, Y. F. Li, W. L. Yu, X. F. Wang, H. C. Sun and B. Yang, *Adv. Funct. Mater.*, 2012, **22**, 4732-4740.
48. L. S. Fan, Y.W. Hu, X. Wang, L. Zhang, F. Li, D. Han, Z. Li, Q. Zhang, Z. Wang and L. Niu, *Talanta*, 2012, **101**, 192-197.
49. J. Shen, Y. Zhu, C. Chen, X. Yang, C. Li, *Chem. Commun.,* 2011, **47**, 2580-2582.
50. S. J. Chen, Y. N. Hong, Y. Liu, J. Z. Liu, C. W. T. Leung, M. Li, R. T. K. Kwok, E. G. Zhao, J. W. Y. Lam, Y. Yu and B. Z. Tang, *J. Am. Chem. Soc.*, 2013, **135**, 4926-4929.
51. F. Yang, M. Zhao, B. Zheng, D. Xiao, L. Wu and Y. Guo, *J. Mater. Chem.*, 2012, **22**, 25471-25479.
52. D. Y. Pan, J. C. Zhang, Z. Li, C. Wu, X. M. Yan and M. H. Wu, *Chem. Commun.*, 2010, **46**, 3681-3683.
53. S. J. Zhu, J. H. Zhang, X. Liu, B. Li, X. F. Wang, S. J. Tang, Q. N. Meng, Y. F. Li, C. Shi, R. Hu and B. Yang, *RSC Adv.*, 2012, **2**, 2717-2720.
54. S. Zhu, J. Zhang, C. Qiao, S. Tang, Y. Li, W. Yuan, B. Li, L. Tian, F. Liu, R. Hu, H. Gao, H. Wei, H. Zhang, H. Sun and B. Yang, *Chem. Commun.*, 2011, **47**, 6858-6860.

55. L. Bao, Z. L. Zhang, Z. Q. Tian, L. Zhang, C. Liu, Y. Lin, B. P. Qi and D. W. Pang, *Adv. Mater.*, 2011, **23**, 5801-5806.

56. J. Zong, Y. Zhu, X. Yang, J. Shen and C. Li, *Chem. Commun.*, 2011, **47**, 764-766.

57. Z. Gan, X. Wu, G. Zhou, J. Shen and P. K. Chu, *Adv. Opt. Mater.*, 2013, **1**, 554-558.

58. K. P. Loh, Q. L. Bao, G. Eda and M. Chhowalla, *Nat. Chem.*, 2010, **2**, 1015-1024.

59. J. Shen, Y. Zhu, X. Yang, J. Zong, J. Zhang and C. Li, *New J. Chem.*, 2012, **36**, 97-101.

60. X. Ran, H. J. Sun, F. Pu, J. S. Ren, X. G. Qu, *Chem. Commun.*, 2013, **49**, 1079-1081.

61. Y. Z. He, X. X. Wang, J. Sun, S. F. Jiao, H. Q. Chen, F. Gao and L. Wang, *Anal. Chim. Acta*, 2014, **810**, 71-78.

62. Z. B. Qu, X. G. Zhou, L. Gu, R. M. Lan, D. D. Sun, D. J. Yu and G. Y. Shi, *Chem. Commun.*, 2013, **49**, 9830-9832.

63. Y. Wang, L. Zhang, R. P. Liang, J. M. Bai and J. D. Qiu, *Anal. Chem.*, 2013, **85**, 9148-9155.

64. L. Zhang, Z. Y. Zhang, R. P. Liang, Y. H. Li and J. D. Qiu, *Anal. Chem.* 2014, **86**, 4423-4430.

65. Y. H. Li, L. Zhang, J. Huang, R. P. Liang and J. D. Qiu, *Chem. Commun.*, 2013, **49**, 5180-5182.

66. X. Li, S. J. Zhu, B. Xu, K. Ma, J. H. Zhang, B. Yang and W. J. Tian, *Nanoscale*, 2013, **5**, 7776-7779.

67. J.J. Liu, X. L. Zhang, Z. X. Cong, Z. T. Chen, H. H. Yang and G. N. Chen, *Nanoscale*, 2013, **5**, 1810-1815.

68. Z. Z. Wu, W. Y. Li, J. Chen and C. Yu, *Talanta*, 2014, **119**, 538-543.

69. J. Zong, X. Yang, A. Trinchi, S. Hardin, I. Cole, Y. Zhu, C. Li, T. Muster and G. Wei, *Biosens. Bioelectron.*, 2014, **51**, 330-335.

70. H. M. Zhao, Y. Y. Chang, M. Liu, S. Gao, H. T. Yu and X. Quan, *Chem. Commun.*, 2013, **49**, 234-236.

71. Z. S. Qian, X. Y. Shan, L. J. Chai, J. J. Ma, J. R. Chen and H. Feng, *Nanoscale*, 2014, **6**, 5671-5674.

72. Z. S. Qian, X. Y. Shan, L. J. Chai, J. R. Chen. and H. Feng, *Nanotechnology*, 2014, **25**, 415-501.

73. Z. S. Qian, X. Y. Shan, L. J. Chai, J. J. Ma, J. R. Chen and H. Feng, *Biosens. Bioelectron.*, 2014, **60**, 64-70.

74. J. Zhao, G. F. Chen, L. Zhu and G. X. Li, *Electrochem. Commun.*, 2011, **13**, 31-33.

75. A. Muthurasu and V. Ganesh, *Biochem. Biotechnol*, 2014, **174**, 945-959.

76. D. L. Jiang, Y. Zhang, H. Y. Chu, J. Liu, J. Wan and M. Chen, *RSC Adv.*, 2014, **4**, 16163-16171.

77. Y. Zhang, C. Y. Wu, X. J. Zhou, X. C. Wu, Y. Q. Yang, H. X. Wu, S. W. Guo and J. Y. Zhang, *Nanoscale*, 2013, **5**, 1816-1819.

78. H. Razmi and R. Mohammad-Rezaei, *Biosens. Bioelectron.*, 2013, **41**, 498-504.

79. X. D. Wang, L. J. Chen, X. R. Su and S. Y. Ai, *Biosens. Bioelectron.*, 2013, **47**, 171-177.

80. L. Wu, J. S. Wang, J. S. Ren, W. Li and X. G. Qu, *Chem. Commun.*, 2013, **49**, 5675-5677.

81. C. Y. Zhang, L. Wang, A. M. Wang, S. Y. Zhang, C. J. Mao, J. M. Song, H. L. Niu, B. K. Jin and Y. P. Tian. *Appl. Surf. Sci.*, 2014, **315**, 22-27.

82. H. M. Yang, W. Y. Liu, C. Ma, Y. Zhang, X. Wang, J. H. Yua and X. R. Song, *Electrochim. Acta*, 2014, **123**, 470-476.

83. Q. Lu, W. Wei, Z. X. Zhou, Z. X. Zhou, Y. J. Zhang and S. Q. Liu , *Analyst*, 2014, **139**, 2404-2410.

84. J. J. Lu, M. Yan, L. Ge, S. G. Ge, S. W. Wang, J. X. Yan and J. H. Yu, *Biosens. Bioelectron.*, 2013, **47**, 271-277.

85. Y. Q. Dong, R. P. Dai, T. Q. Dong, Y. W. Chi and G. N. Chen, *Nanoscale*, 2014, **6**, 11240-11245.

86. N. Chen, Y. He, Y. Su, X. Li, Q. Huang, H. Wang, X. Zhang, R. Tai and C. Fan, *Biomaterials*, 2012, **33**, 1238-1244.

87. M. C. Mancini, B. A. Kairdolf, A. M. Smith and S. Nie, *J. Am. Chem. Soc.*, 2010, **130**, 10836-10837.

88. X. H. Gao, L. L. Yang, J. A. Petros, F. F. Marshal, J. W. Simons and S. M. Nie, *Curr. Opin. Biotechnol.*, 2005, **16**, 63-72.

89. R. Hardman, *Environ. Health Perspect.*, 2006, **114**, 165-172.

90. P. J. Fairchild, K. F. Nopan, S. Cartland and H. Waldmann, *Int. Immunopharmacol.*, 2005, **5**, 13-21.

91. D. J. Prockop, *Science*, 2001, **293**, 211-212.

92. G. C. Parker, M. Nastassova-Kristeva, L. M. Eisenberg, M. S. Rao, M. A. Williams, P. R. Sanberg and D. English, *Stem Cells Dev.*, 2005, **14**, 463-469.

93. A. Solanki, J. D. Kim and K. B. Lee, *Nanomedicine*, 2008, **3**, 567-578.

94. Y. E, L. Bai, L. Fan, M. Han, X. Zhang and S. Yang, *J. Mater. Chem.*, 2011, **21**, 819-823.

95. W. Shang, X. Zhang, M. Zhang, Z. Fan, Y. Sun, M. Han and L. Fan, *Nanoscale*, 2014, **6**, 5799-5806.

96. Z. Qian, J. Ma, X. Shan, L. Shao, J. Zhou, J. Chen, and H. Feng, *RSC Adv.*, 2013, **3**, 14571-14579.

97. X. Zhu, X. Xiao, X. Zuo, Y. Liang and J. Nan, *Part. Part. Syst. Charact.*, 2014, **31**, 801-809.

98. C. Hu, Y. Liu, Y. Yang, J. Cui, Z. Huang, Y. Wang, L. Yang, H. Wang, Y. Xiao and J. Rong, *J. Mater. Chem. B*, 2013, **1**, 39-42.

99. S. Chen, X. Hai, C. Xia, X.-W. Chen and J.-H. Wang, *Chem. Eur. J.*, 2013, **19**, 15918-15923.

100. N. Li, X. Liang, L. Wang, Z. Li, P. Li, Y. Zhu and J. Song, *J. Nanopart. Res.*, 2012, **14**, 1177-1185.

101. W. J. Xie, Y. Y. Fu, H. Ma, M. Zhang and L. Z. Fan, *Acta Chimica Sinica*, 2012, **70**, 2169-2172.

102. H. Sun, L. Wu, N. Gao, J. Ren and X. Qu, *ACS Appl. Mater. Interfaces*, 2013, **5**, 1174-1179.

103. V. Kumar, V. Singh, V. Umrao, V. Parashar, S. Abraham, A. K. Singh, G. Nath, P. S. Saxena and A. Srivastava, *RSC Adv.*, 2014, **4**, 21101-21107.

104. L. Zhang, Y. Xing, N. He, Y. Zhang, Z. Lu, J. Zhang and Z. Zhang, *J. Nanosci. Nanotechno*, 2012, **12**, 2924-2928.

105. J. Nicolas, S. Mura, D. Brambilla, N. Mackiewicz and P. Couvreur, *Chem. Soc. Rev.*, 2013, **42**, 1147-1235.

106. M. Shi, J. Lu and M. S. Shoichet, *J. Mater. Chem.*, 2009, 19, 5485-5498.

107. X. Sun, Z. Liu, K. Welsher, J. Robinson, A. Goodwin, S. Zaric and H. Dai, *Nano Res.*, 2008, **1**, 203-212.

108. P. Nigam, S. Waghmode, M. Louis, S. Wangnoo, P. Chavan and D. Sarkar, *J. Mater. Chem. B*, 2014, **2**, 3190-3195.

109. X. Wang, X. Sun, J. Lao, H. He, T. Cheng, M. Wang, S. Wang and F. Huang, *Colloid. Surface. B*, 2014, **122**, 638-644.

110. X. T. Zheng, A. Than, A. Ananthanaraya, D.-H. Kim and P. Chen, *Acs Nano*, 2013, **7**, 6278-6286.

111. J.-L. Li, H.-C. Bao, X.-L. Hou, L. Sun, X.-G. Wang and M. Gu, *Angew. Chem., Int. Ed.*, 2012, **51**, 1830-1834.

112. S. T. Yang, L. Cao, P. G. Luo, F. Lu, X. Wang, H. Wang, M. J. Meziani, Y. Liu, G. Qi and Y. P. Sun, *J. Am. Chem. Soc.*, 2009, **131**, 11308–11309.

113. H. Tao, K. Yang, Z. Ma, J. Wan, Y. Zhang, Z. Kang and Z. Liu, *Small*, 2012, **8**, 281–290.

114. P. G. Luo, S. Sahu, S.-T. Yang, S. K. Sonkar, J. Wang, H. Wang, G. E. LeCroy, L. Cao and Y.-P. Sun, *J. Mater. Chem. B*, 2013, **1**, 2116-2127.

115. L. Cao, S. T. Yang, X. Wang, P. G. Luo, H.-H. Liu, S. Sahu, Y. Liu and Y. P. Sun, *Theranostics*, 2012, **2**, 295-301.

116. K. Yang, S. Zhang, G. Zhang, X. Sun, S.-T. Lee and Z. Liu, *Nano Lett.*, 2010, **10**, 3318-3323.

117. Y. Jing, Y. Zhu, X. Yang, J. Shen and C. Li, *Langmuir*, 2010, **27**, 1175-1180.

118. A. Zhu, C. Ding and Y. Tian, *Sci. Rep.*, 2013, **3**, 2933-2939.

119. J. Zong, X. Yang, A. Trinchi, S. Hardin, I. Cole, Y. Zhu, C. Li, T. Muster and G. Wei, *Nanoscale*, 2013, **5**, 11200-11206.

120. G. Hong, J. C. Lee, J. T. Robinson, U. Raaz, L. Xie, N. F. Huang, J. P. Cooke and H. Dai, *Nat. Med.*, 2012, **18**, 1841-1846.

121. N. Vogt, *Nat. Meth.*, 2014, **11**, 988-989.

122. A. M. Smith, M. C. Mancini and S. Nie, *Nat. Nano.*, 2009, **4**, 710-711.

123. *Nature*, 2014, **512**, 117-117.

124. G. Hong, S. Diao, J. Chang, A. L. Antaris, C. Chen, B. Zhang, S. Zhao, D. N. Atochin, P. L. Huang, K. I. Andreasson, C. J. Kuo and H. Dai, *Nat. Photon*, 2014, **8**, 723-730.